Biomineral structure and crystallographic arrangement of cerioid and phaceloid growth in Syringoporicae corals (Tabulata, Devonian-Carboniferous): a genetic reflection

Ismael Coronado[1], Sergio Rodríguez [1,2]

[1] *Departamento de Paleontología, Universidad Complutense de Madrid. C/ José Antonio Nováis 12, Ciudad Universitaria. E-28040 Madrid. Spain.* ismael.coronado@geo.ucm.es

[2] *Instituto de Geociencias (IGEO. CSIC-UCM). C/ José Antonio Nováis 2, Ciudad Universitaria. E-28040 Madrid. Spain.*

Short title: *Biomineralization of cerioid-phaceloid corals.*

Abstract: An extensive study of the microstructure, nanostructrure and crystallographic properties of six taxa belonging to four different genera of Devonian and Carboniferous Syringoporicae, showing dense phaceloid (*Pleurosiphonella*), pseudoceriod (*Neomultithecopora*) and cerioid (*Roemeria* and *Roemeripora*) has been done in order to disclose the similarities and differences of the growth processes at biomineral scale and understand the growth processes that provide organisms with an evolutionary advantage to colonize different habitats. The techniques used for this purpose are: petrographic microscopy, scanning electron microscopy (SEM), atomic force microscopy (AFM) and computer-integrated polarization microscopy (CIP). Micro- and nanotextural features are common in all of skeletons studied, showing that they were composed of hierarchical structures. All studied taxa are composed of a complex nanostructure composed of co-oriented rounded nanocrystals with different sizes and morphologies, depending on the taxon. The identified microstructures include granulae, lamellae, fibres and hyaline elements. The crystallographic techniques demonstrated that all of them except hyaline elements are biogenic in origin. The granules could be

aborted fibres during the growth of two corallites in contact. The Syringoporicae skeletons are a product of matrix-mediated biocrystallization. The data reveal that the skeleton structure is a reflection of the genetic code. The median lamina is formed by the joint crystallization of both polyps at the same time. The variation in the internal structural organization (phaceloid, pseudocerioid or cerioid) is conditioned by the environment; on the contrary, the final structure is controlled by genetics.

Keywords: biocrystallization processes, Palaeozoic corals, calcite, bio-composite.

1. Introduction

Biologically controlled minerals form part of innumerable organisms (both unicellular and multicellular). These biominerals (*sensu* Marin *et al*., 2014), composed of a mixture between inorganic and organic phases, form shells and skeletons of terrestrial and aquatic organisms, which have specific biological functions (support, protectionfrom predators, defence against chemical agents, feeding, senses etc…) and structures (teeth, bones, shells, plates, spines, otoliths…). These frames are composed of biominerals which stand out by specific crystallochemical properties (Mann, 2001) such as: "*uniform particle sizes, well defined structures and compositions, high levels of spatial organization, complex morphologies, controlled aggregation and texture, preferential crystallographic orientation and higher-order assembly* (known as self-assembly) *into hierarchical structures"*. Biominerals are present in the marine realm as incalculable forms and compositions, with calcium carbonate ($CaCO_3$) one of the most representative. Aragonite, calcite and vaterite are ubiquitous minerals in shells, skeletons or skeletal elements of marine organisms (such as molluscs, corals, brachiopods, algae, coccoliths, ascidians…) and each group of organisms (Stolarski, 2000; Mann, 2001; Berman, 2010; Cusack *et al*., 2008; Taylor, 2008; Frýda *et al*., 2010)

have different crystal shapes, sizes and distributions (microstructure *sensu* Checa *et al*. (2013). The microstructure of each calcifying organism may be formed by crystals of a single mineralogy or by multiple phases, different morphologies and arrangements of crystals. The new insights on biomineralization techniques have allowed evaluating and analysing the crystallographic orientation of each microstructure (their preferential texture) and discovering their assembly processes (Pérez-Huerta & Cusack, 2008; Benzerara *et al*., 2011; Checa *et al*., 2013). New scales of study have been explored, with the development of new microscopy techniques, shedding light on the hierarchical composition of the frameworks, from nanoscale (nanocrystals and organic coatings) to macroscale (shell and skeletons).

All these properties and characteristics are controlled by the organic phases (e.g. macromolecular framework, Lowenstam & Weiner, 1989; Mann, 2001; Cuif *et al*., 2011) secreted by the mineralizer cells, which play an important role in biomineralization (e.g., in molluscs and corals; Cuif *et al*., 1999, Dauphin *et al*., 2002). The main controlling mechanisms in biomineralization processes are governed by a gene pool (*sensu* Mann, 2001), which are conditioned by bioenergetic processes and adapted to environmental influences. The main controlling mechanisms *sensu* Mann (2001) are chemical (ion transport, saturation), spatial (confining processes of supramolecular organization), structural (preferential nucleation), morphological (morphogenesis) and constructional (higher-order structures).

The distinctive properties of biominerals may be detected and analysed in the fossil record if and when diagenetical processes have not obliterated the original attributes. The importance of biomineralization studies in fossils can help our understanding of the evolution of metazoans through the Phanerozoic. Biominerals offer chemical information about the environmental conditions where they were precipitated (by

74 geochemical proxies), but also, they offer a single unique position to understand the
75 growth processes that provide organisms with an evolutionary advantage to colonize
76 different habitats (e.g., growth patterns, Barbin *et al*., 2008; changes in their
77 mineralogy, Stolarski *et al*., 2007, Balthasar *et al*., 2011; formation of structural
78 elements, Pérez-Huerta *et al*., 2009). Recent articles have developed these focuses in
79 different fossil groups, such as molluscs (Frýda *et al*., 2009; Clark II, 1999; Dauphin,
80 2002), brachiopods (Balthasar *et al*., 2011; Pérez-Huerta *et al*., 2007; Tomašových &
81 Farkaš, 2005), cnidarians (Stolarski, 2003; Stolarski *et al*., 2007; Gautret, 2000; Vinn &
82 Kirsimäe, 201X), poriferans (Cuif *et al*., 2011) and trilobites (Lee *et al*., 2012; Torney
83 *et al*., 2014).

84 Thus, biomineralization studies of Palaeozoic corals have been historically centred in
85 the analysis of microstructures from a taxonomical point of view as an important
86 character (Ogilvie, 1895; Wang, 1950; Brood, 1978; Semenoff-Tian-Chansky, 1984;
87 Sorauf, 1984; Rodríguez, 1989; Lafuste and Plusquellec, 1990) or from their
88 preservation state. This last point has been the subject of controversy for more than 70
89 years (see Coronado *et al*., 2013; Rodríguez, 1989 for a review). Currently, new
90 advances on biomineralization of Palaeozoic corals have been focused on the biogenic
91 origin of skeletons of Carboniferous Syringoporicae (Coronado *et al*., 2013; Coronado
92 *et al*., 2014a; Coronado *et al*., 2014b) a superfamily of tabulate corals (Coronado &
93 Rodríguez, 2014). A complete assessment of the biogenic origin of microstructures was
94 done by Coronado *et al*. (2013) by the use of a combination of techniques (petrography
95 microscopy; scanning electron microscopy, SEM; atomic force microscopy, AFM;
96 electron-backscatter diffraction, EBSD; cathodoluminescence, CL; electron microprobe
97 analysis, EMPA), which allow to observe the main properties of microstructures of
98 *Multithecopora hontoriense*. The study revealed that the skeletons are formed by

hierarchical structures from nanoscale to macroscale. Coronado *et al*. (2014b) studied by EBSD the preferred crystallographic orientations in different microstructural elements, the processes of growth of skeletons and development of wall elements in seven taxa of Syringoporicae corals. A subsequent study (Coronado *et al*., 2014a) of other Syringoporicae (*Sinopora*) was done to establish a technique (computer-integrated polarization, CIP) applied to the study of crystallographic organization of biominerals and focused on diagenetical aspects, which in combination with SEM, AFM and CL allowed to characterize the original properties of skeletons. These studies have denoted the biogenic origin of microstructures of Syringoporicae corals, providing light on growth processes, the assembly mechanisms and those abiogenic characteristics specific to diagenetical alteration of these microstructures.

1 .a. Structure of the colony of Palaeozoic corals

Palaeozoic corals are solitary and colonial cnidarians that inhabited Palaeozoic seas from early Ordovician to Permian. Within this informal group the most abundant orders in the fossil record are Tabulata and Rugosa. Tabulata are considered to be entirely colonial (Scrutton 1997) whereas part of Rugosa are solitary (Scrutton, 1998). Scrutton (1988) differentiated between growth-form and the internal structural organization of corallum, which forms the complete compound skeleton (Hill, 1981). The external appearance of the colony is the growth-form (fasciculate, cateniform, retiform, umbelliferous, massive, ramose and foliose *sensu* Scrutton, 1998). The internal structural organization indicates the interrelationship of modules (corallites) within the the corallum (dendroid, phaceloid, cerioid, amural or plocoid and coenenchymal *sensu* Scrutton, 1998). This variety of forms, and in some cases, the integration of some of them in the same corallum suggest a great plasticity in the Palaeozoic coral skeletons making it very difficult to determine the level of colonial integration, and generating a

high intraspecific variation in corals. This intraspecific variation may be controlled by a genotypic or a phenotypic response and even, in some cases, by an ecophenotypic response. Scrutton (1988) describes six kinds of variations (ontogenetic, astogenetic, cyclomorphic, topomorphic, disturbance and pathological), thus making it very difficult to differentiate by the study of skeletons.

In this way, the biomineralization studies may help to recognize some characteristics that only can be controlled by genetic code. As mentioned above, the controlled biominerals are an expression of the cellular mineralizer tissues, so the crystallochemical properties of biominerals are controlled by genotype and those variations in the growth-form or internal structural organization, due to environmental fluctuations, should be regulated by the genetic code because they vary in each taxon.

Syringoporicae are composed of fasciculate, massive and cateniform coralla with a variable internal structural organization, being most commonly phaceloid and dendroid and less commonly cerioid or pseudocerioid (Tchudinova, 1986; Poty, 2010; Coronado *et al*., 2014b). Coralla with intraspecific variation are common in this superfamily (e.g. cerioid-phacelloid). Tchudinova (1986) remarks that the final growth-form of Syrigoporicae is strongly influenced by the genetic strategy and the environment.

Cerioid and pseudocerioid coralla are found in several genera of Multithecoporidae, Roemiriidae, Tetraporellidae and Thecostegitidae families. Coronado *et al*., (2014b) observed during the study of *Roemeripora* sp. skeletons in which the crystallographic arrangement of the cerioid taxa (with shared-walls and prismatic corallites) differs from the phaceloid taxa with cylindrical corallites (i.e. *Multithecopora*, *Syringopora* and *Sinopora*), even keeping common crystallographic properties. Several authors have described intraspecific variation from cerioid to phaceloid stages in the same corallum

148 (e.g., Tchudinova, (1986) in *Duncanopora*; Lafuste & Tourneur (1988a) and Tourneur
149 & Lafuste (1991) in *Roemeria;* Coronado & Rodríguez (2014) in *Neomultithecopora*).

150 An evolutionary study of Syringoporicae (Tchudinova, 1986) revealed that although the
151 first appearance of the group is in the Middle Ordovician with *Syringoporinus,* a
152 cateniform to cerioid corallum with cylindrical-prismatic corallites (Tchudinova, 1986),
153 the trend during the evolution of Syringoporicae is towards forming phaceloid coralla
154 having cylindrical corallites (Tchudinova, 1980). Thus, intraspecific variation in the
155 internal structure of the corallum and the growth-form (cerioid to phaceloid, massive to
156 fasciculate) are diverse and depend on the taxa. Some coralla of *Multithecopora*
157 *hontoriense* change their corallum morphology during environmental fluctuations,
158 varying the corallites distance, packing them together, but maintaining the phaceloid
159 structure with cylindrical or irregular corallites (Coronado & Rodríguez, 2014); whereas
160 *Roemeria* (Lafuste & Tourneur, 1988a) and *Neomultithecopora* (Coronado &
161 Rodríguez, 2014) change their internal structural organization from phaceloid to cerioid
162 or pseudocerioid, with prismatic corallites. This suggests that morphological
163 intraspecific variation could be exerted by the environmental conditions, but in the case
164 of variations in the internal structural organization, should be controlled by genetics.

165 This study presents a detailed structural and crystallographic analysis of six taxa
166 belonging to four different genera of Devonian and Carboniferous Syringoporicae,
167 which are phaceloid with shared walls (*Pleurosiphonella*, Fig. 1), cerioid (*Roemeria* and
168 *Roemeripora*, Fig. 1, 2) and pseudoceriod (*Neomultithecopora*, Fig. 2). The purpose of
169 this work is to disclose the similarities and differences of the growth processes at
170 biomineral scale, between cerioid and phaceloid taxa and finally to study the
171 architectural adaptations derived from environmental fluctuations.

2. Material

The Devonian material studied in this research is part of the Lafuste´s collection of the Muséum National d'Histoire Naturelle (MNHN) from Paris (France): The samples belong to the species *Roemeria bohemica* Počta, 1902 (Fig. 1a-b), Pragian in age (A47624) (details on the locality in Tourneur & Lafuste, 1991); *Roemeria cubinensis* Lafuste & Tourneur, 1988a (Fig. 2H-I), Eifelian in age (A47625) and *Roemeria infundibulifera* (Goldfuss 1829) (Fig. 2f-g), Givetian in age (A47626) (details on the locality of two last taxa in Lafuste & Tourneur, 1988a).

The Carboniferous material comes almost entirely from the collection of the Universidad Complutense of Madrid (Spain) and it consists of two taxa: *Roemeripora* sp. (Fig. 1c-d) from Fuenteobejuna section (upper Viséan, details in Coronado & Rodríguez, 2014a), and *Neomultithecopora cantabrica* Rodríguez & Ramírez, 1987 from Prioro (PR) (Fig. 2d-e) and Playa de la Huelga sections (HO) (Fig. 2a-c), upper Moscovian in age (details in Coronado and Rodríguez, 2014a),. The genus *Roemeripora* was considered as a synonym of *Roemeria* by Tourneur & Lafuste (1991), but in this article it will be considered as a different genus. Additionally, some cateniform samples of *Pleurosiphonella* Tchudinova, 1970 having phaceloid corallum with shared walls (Fig. 1e-f) from of the Lafuste´s collection of the Muséum National d'Histoire Naturelle (MNHN) from Paris (France) have been studied (A47627). These samples were collected in 1979 by Dr. G. A. Gill in the Viséan of Czatkowice (Poland) and the taxonomical characterization (*Pleurosiphonella* sp.) was done by Dr. J. Lafuste. Precisions in the location of samples are unknown.

3. Methods

For the purpose of checking the structural and crystallographic properties of each skeleton, a combination of different techniques have been applied, including petrographic microscopy, scanning electron microscopy (SEM), atomic force microscopy (AFM) and computer-integrated polarization microscopy (CIP). The structural level has been studied at two different scales: at nanoscale (AFM) and at microscale (SEM and petrographic microscopy), although only four taxa from five localities (*Roemeria bohemica*, *Roemeripora* sp., *Neomultithecopora cantabrica* (PR and HO) and *Pleurosiphonella* sp.) have been studied under AFM because some samples of MNHN as rocks slabs were unavailable or the thin sections were covered with resin. Microscale structures have been studied with petrographic microscopy and ultrathin sections (UTS) of all taxa but only in *Roemeripora* sp. SEM has been used to study the inner structure of microcrystals. Computer-integrated-polarization microscopy (CIP) was used for recognising the crystallographic arrangement of the skeletons of all taxa.

3. a. S*tructural characterisation*

Petrographic microscopy, SEM and AFM were used for visualisation and characterisation of the microstructures and nanotextures of selected taxa. Ultra-thin sections were prepared in *Roemeripora* sp. and *Neomultithecopora cantabrica* with the method developed by Lafuste (1970), to correct visualization of microcrystals under petrographic microscopy. Longitudinal and transverse sections of *Roemeripora* sp. were broken by means of natural breakage. Details of the methods and equipment used can be found in Coronado *et al*. (2013, 2014a).

3. b. Crystallographic characterization

Ultra-thin sections (transverse and longitudinal) of all taxa were used for CIP analysis, independently of the preparation method of UTS (cover or uncovered). The CIP method (computer-integrated-polarization microscopy) has been described by Heilbronner *et al*. (1993), Heilbronner (2000), and Heilbronner & Barret (2014) as a method for texture analysis and optical orientation imaging. It determines the *c*-axis orientations of uniaxial minerals from optical micrographs and displays the results in the form of pole figures and orientation images, using a colour-code (CLUT), which represents each orientation. This method has been applied to biomineralization studies of fossil specimens with relevant results (Coronado *et al*., 2014a). Details of the methods and equipment used can be found in Coronado *et al*. (2014a). The petrographic micrograph and the CIP analyses have been done with Image SXM software (Barret, 1997).

FIGURE 1

4. Results

4. a. Structure of skeletons

The taxa selected have different growth-forms and internal structural organizations. *Roemeria bohemica* (Fig. 1a-b), *R. cubiniensis* (Fig. 2h-i), *R. infundibulifera* (Fig. 2f-g) and *Roemeripora* sp. (Fig. 1c-d) show massive cerioid colonies, with prismatic corallites (four-six sides) and dome shape of colony. In the cases of *R. cubiniensis and R.infundibulifera* some colonies show an alternating internal structural organization between cerioid-pseudoceriod-phaceloid in some points of the colony (cylindrical corallites) such as peripheral areas (Lafuste and Tourneur, 1988a), although only the cerioid areas have been studied in these samples. Tourneur & Lafuste (1991) describe the same habit in some colonies of *R. bohemica*. On the other hand, *Neomultithecopora cantabrica* (Fig. 2a-e) shows a variable internal structural organization depending on

242 their position in the colony. The beginning of growth is phaceloid prostrated attached to
243 hard substrates such as chaetetids (cylindrical corallites, Fig. 2a, e) and secondarily the
244 corallites growth is erect by lateral increase over this initial stage (Fig. 2b,e). During the
245 growth the corallites are aggregated in a massive colony passing from a phaceloid
246 internal structure to cerioid (prismatic corallites), mainly in the wave zone of the colony
247 (Fig. 2c-d). The shadow-zone and some peripheral areas continued growing with
248 phaceloid development. Ultimately, *Pleurosiphonella* sp. shows a phaceloid internal
249 structure with halysitid-type corallites, oval section, and cateniform shape of colony
250 (Fig. 1e-f).

251 FIGURE 2

252 The microstructure of skeletons of Syringoporicae is composed of a framework of
253 concentric alternating domains of calcite crystals (Fig. 3, 4), whose main morphologies
254 are: lamellae, fibres and granules. These three microstructural elements have been
255 identified in studied taxa. Details of domains, which make up the skeleton, their
256 position and the dimensions of each microstructural element in each taxon, have been
257 summarized in Table 1.

258 Lamellae, > 25 μm in size, and microlamellae, < 25 μm in size (Rodríguez, 1989) are
259 single crystals straight to wavy, with indentations at their edges and flake forms. The
260 morphologies are variable and depend on their position in the skeleton (*i.e.* the contact
261 with other microstructural element) and the taxa. They can be 'scutellate' or shield-
262 shape (Lafuste, 1985); cupolar-shape; 'tenailles' or pliers-shape (Lafuste, 1983);
263 'lunular' or moon-shape (Lafuste, 1978) and geniculate-shape (Lafuste, 1981). In this
264 article we will not make distinction of morphology, considering only lamellae and
265 microlamellae, but some examples of these morphologies can be found in the Figures 3

and 4. These elements are completely imbricated with each other forming a compact framework (Fig. 3, 4). The morphological axis is oriented perpendicular to the lumen and the concave part of lamellae always points to the lumen, showing a concentric aspect of the lamellar domains (Fig. 3, 4). These elements have a great lateral development in two dimensions; their length varies from 7 to 46 μm, and their width fluctuates from 2 to 11 μm depending on the taxon (Table 1). Most skeletons of taxa studied here have microlamellae except *Roemeria infundibulifera*, *Roemeria cubiniensis*, the lamellar external domain of *Roemeria bohemica* and *Neomultithecopora cantabrica*. Natural breakage of the corallites of *Roemeripora* sp. shows that the lamellae are composed of submicrometric intralamination almost parallel to the morphological axis of the lamella independent of their wavy surface or lateral wedging (Fig. 4g-h).

TABLE 1

Fibres are elongated crystals with irregular morphology, indentations in their edges and an apex or tip at the end and sometimes at the base. Similar to lamellae, the morphology is variable; strip-shape or palisade, barrel-shape, irregular elongated-shape and tabular-shape, depending on their position in the skeleton. The morphological axis is oriented towards the lumen, parallel to the direction of growth. Irregular elongated shape fibres appear in the holacanth septal spines of several studied taxa *Roemeripora* sp. and *Roemeria bohemica*. Their length varies from 8 to 70 μm, and their width fluctuates from 1 to 14 μm depending on the taxon (Table 1) and morphology.

FIGURE 3

'Granules' are single crystals with indentations to their edges and a round flake-shape. They have irregular sizes with lengths from 2 to 51 μm, and their width fluctuates from

290 2 to 29 μm. Two kinds of granules can be recognized in the studied taxa. Short,
291 irregular, equidimensional and with low variability of sizes (*Roemeripora* sp. and
292 *Neomultithecopora cantabrica*), known as granules (*sensu* Lafuste & Plusquellec,
293 1988), and a second kind of large granule, asymmetric and with high variability of sizes
294 and morphologies (*Roemeria bohemica*, *R. infundibulifera* and *R. cubiniensis*), known
295 as hyaline elements (*sensu* Lafuste & Tourneur, 1990). This last element has been
296 described as elongated granules (Lafuste & Plusquellec, 1986), hyaline stelloid-shape
297 (Lafuste & Tourneur, 1988a), platelets (Lafuste & Tourneur, 1988b), long hyaline
298 elements (Lafuste & Tourneur, 1990), sticks ('baguette', Lafuste & Tourneur, 1991b)
299 and ribs (Lafuste *et al*., 1992). Hyaline elements are characteristic of irregular
300 surrounded morphologies in all *Roemeria* taxa as well as hyaline stelloid-shape crystals
301 in *R. cubiniensis* and 'baguettes' and hyaline stelloid-shape crystals in *R. bohemica.* It
302 should be taken into account that some of these asymmetric crystals have opaque
303 impurities inside. Both 'granules' (equidimensional granules and hyaline elements) are
304 situated in the median lamina. The median lamina is a black 'line' under transmitted
305 light microscopy first described by Nicholson (1879) and it has been interpreted as an
306 irregular (even dashed) crystal domain of secretion of polyps between two edges of
307 skeletons (Plusquellec, 1976; Plusquellec & Tchudinova, 1977). This lamina has been
308 described in the middle of septa and shared-walls in colonial forms of rugose and
309 tabulate corals. Their dark appearance is related to the distribution and size of granules
310 and their degree of imbrication; which cannot allow light transmission and it only can
311 be observed using UTS in petrographic microscopy or SEM.

312 FIGURE 4

313 Noteworthy, is a gradual change between the fibrous and lamellar domains, with the
314 modification of the regular shapes (shield-shape lamellae and elongated fibres) by

315 intermediate shapes, as was described above (cupolar-shape; pliers-shape), independent
316 of the internal structure of colony. This gradual transition between the microcrystals can
317 be observed also between the granules and lamellae in *Roemeripora* sp. or
318 *Neomultithecopora cantabrica,* but it cannot be seen in the transition to lamellae or
319 fibres and the hyaline elements (e.g. *Roemeria bohemica, R. infudibulifera or R.*
320 *cubiniensis*). The median lamina formed by hyaline elements lacks continuity, with a
321 disrupted or dashed development versus the wavy path of the granular median lamina in
322 *Roemeripora* and *Neomultithecopora*. The granular median lamina of *Roemeripora* sp.
323 changes during the growth of corallites and their widening. The granular domain
324 changes to an external fibrous domain. This process is known 'fibrerization' of the
325 median lamina (Lafuste *et al*., 1992) in other massive tabulate corals. A similar process
326 can be observed in *R. cubiniensis* (Fig. 3h) where the widening process of corallites
327 allow to develop a fibrous domain with elongated fibres in the place of median lamina.

328 *Pleurosiphonella* sp. skeletons show halysitid morphology (sometimes oval) of the
329 corallites in their growth of cateniform colony. During the lateral increase (Fig. 1e) the
330 corallites grew straight over the substrate and sometimes they shared the wall in those
331 points where the connecting structures (connecting tubules, Fig. 1e) are formed,
332 changing from cylindrical to oval corallites. This process of growth generated a shared-
333 wall structure between two corallites in which the microstructure was flattened and their
334 path was conditioned to the morphology of connecting structure as if the polyps were
335 stretched during the secretion of skeleton. The morphological axis of microcrystals in
336 the symmetric plane along the connecting structure is abruptly turned and the transition
337 between two corallites is a net contact.

338 The microcrystals of Syringoporicae studied with AFM (*Roemeripora* sp., *Roemeria*
339 *bohemica*, *Pleurosiphonella* and *Neomultithecopora cantabrica*) reveals that they are

340 composed of a complex nanostructure composed of co-oriented rounded nanocrystals
341 with different sizes and morphologies, which depend on the taxon.

342 FIGURE 5

343 *Roemeripora* sp. microcrystals (lamellae and fibres) are composed of an aggregate of
344 nanogranules with variable sizes, 30–116 nm (x = 62 nm) in length, 22-97 nm (x = 44
345 nm) in width. They are disposed forming nanolaminae ~50 nm thick and they in turn are
346 forming submicrometric structures (intralamination) of ~300 nm. Both, nanocrystals
347 and nanolaminae are surrounded by dark colour envelopes, as the phase images show
348 (Fig. 5a, c-e). These envelopes are easily observable in amplitude images (Fig. 5a, d)
349 because they produce a positive relief around the nanocrystals, inasmuch as the
350 amplitude images are the measure of deflection of the tip with the topography of the
351 sample providing information of the topography of the sample. Each granule is
352 surrounded by a thin envelope 3–16 nm in thickness, depending on their positions in the
353 microcrystals. This intralamination corresponds with the submicrometric
354 intralamination observed by SEM in the microcrystals (Fig. 4g-h). *Roemeria bohemica*
355 has a nanotexture that shows an aggregate of irregular, co-oriented, pill-shape
356 nanogranules (Fig. 5h-i), which show variable sizes 17–72 nm (x = 38 nm) in length,
357 13-45 nm (x = 25 nm) in width. They are similar to those described by Coronado *et al*.
358 (submitted) for *Syringopora* but these have a smaller size. The nanogranules show a
359 thin dark envelope (Fig. 5i), less marked than *Roemeripora* sp. 3-5 nm in thickness.
360 Some areas of microcrystals have evidences of nanogranules fusion, forming larger
361 units (Fig. 5f, black arrows). In those edges between co-oriented microcrystals points or
362 surfaces of contact can be observed (Fig. 5g, black arrow) with the nanounits co-
363 oriented. *Pleurosiphonella* sp. microcrystals are composed of aggregates of
364 subquadrangular nanogranules with surrounded corners (Fig. 6b-c) of variable sizes 28–

93 nm (x = 52 nm) in length, 27-52 nm (x = 35 nm) in width, which are arranged in nanolaminae, similar to *Roemeripora* sp. These nanolaminae are stacked forming larger units of submicrometric intralamination (Fig. 6b), similar to those described in *Roemeripora* sp. Taking in account that the etching has been the same in the entire sample, it should be highlighted the differential etch produced in the contact of microcrystals (Fig. 6a, d). In those contacts between co-oriented microcrystals, the etching has not been completed between them, showing some points with co-oriented nanocrystals in contact (Fig. 6a). On the other hand, those misoriented microcrystals have a deeper etching in the contact between crystals (Fig. 6d), without contact points. The nanolamination allows observing clearly the misorientation between microcrystals. Figure 6d shows a contact between two lamellae and a misorientation of ~30° can be observed (double arrow lines). The nanogranules show a dark envelope of 5.5–23 nm thickness (Fig. 6c), and they have a higher thickness in the contact between nanolaminae (Fig. 6c, white arrow), as occurs in *Roemeripora* sp. As a last example, the structure of microcrystals in *Neomultithecopora cantabrica* have been studied in samples from different localities with a similar age. The structure to nanoscale of *N. cantabrica* is characterized by an aggregation of irregular elongated nanogranules (ellipsoidal-shape) (Fig. 6g, k), arranged in nanolaminae (Fig. 6f, i-j) with their morphological axis oblique to the plane of accretion (Fig. 6g). The inner structure of these nanolaminae are composed of a stack of nanogranules and in turn the nanolaminae are stacked composing higher structures, similar to submicrometric intralamination 200-500 nm in thickness, as was emphasised in previous taxa. The sizes are variable and slightly different between two samples, although this can be interpreted as intraspecific variation. Hontoria samples have 27–93 nm (x = 56 nm) in length, 21-93 nm (x = 43 nm) in width, whereas Prioro samples have 26–98 nm (x = 51 nm) in length, 18-60 nm

390 (x = 35 nm) in width. The elongated nanogranules show a thin dark envelope (Fig. 6h, l)
391 around them 3-7 nm in thickness.

392 FIGURE 6

393 **4. b. Crystallographic arrangement**

394 Computer-integrated-polarization microscopy (CIP) has been used in all studied taxa
395 with the purpose of identify the crystallographic arrangement of the skeletons. Ten c-
396 axis orientation images (COI) and their corresponding pole-figures were obtained using
397 the CIP method from different shared-walls and phaceloid corallites. Some
398 considerations should be taken into account before beginning the description of the
399 studied taxa. The diagenetical alteration can be mapped with crystallographic methods
400 (including CIP) in polycrystalline skeletons, as has been shown by some authors (Pérez-
401 Huerta *et al*., 2007, 2012; Coronado *et al*., 2013, 2014a, 2014b; Moreno-Azanza *et al*.,
402 2013). Well-structured frameworks produced by controlled biomineralization, such as
403 skeletons and shells, show a great crystallographic control. During the diagenetical
404 alteration, the crystallographic axis lose the original properties (azimuth and/or
405 inclination) and the new crystals (in frameworks), formed by processes of
406 dissolution/precipitation, usually show a random orientation pattern. Black dots and
407 black areas in orientation images correspond with those areas with artefacts derived by
408 scratches or dust in the UTS, which have been removed from the analysis.

409 FIGURE 7

410 *Roemeripora* sp. has been studied in a slightly oblique transverse section (Fig. 7a-c) and
411 a transverse section of a thickened corallite from a more calicular region (Fig. 7d-f). The
412 oblique region in the contact of two corallites is separated by a wavy granular median
413 lamina ~55 μm in thickness (fig. 7a). In the petrographic micrograph and orientation

414 image three main areas can be identified (two lamellar domains and a median lamina),
415 which show different orientations of c-axis. An irregular mixture of microlamellae (e.g.
416 geniculated, cupolar) is present in the sclerenchyma in both walls, which appear to be
417 arranged in rows (Fig. 7a-b), regarding to fibres. As in the transverse section, the c-axis
418 is oriented perpendicular to their morphological axis. The c-axis in the lamellae of the
419 oblique section has an inclination of ~60-65° (Fig. 7c) in both walls, whereas the
420 inclination of c-axis of granules of the median lamina is ~75-90° (Fig. 7c). The c-axis
421 inclination in the left wall is ~30° near of lumen. The azimuth of c-axis of both walls is
422 misoriented ~60°. The orientations (azimuth) of the granular zone are composed of a
423 mixture of orientations (azimuth) belonging to both walls, in which is revealed by the
424 blue-yellow and green colouration of the orientation image. The petrographic
425 micrograph of the transverse section (Fig. 7d) shows two microlamellar walls separated
426 by a fibrous median lamina of ~75 μm thickness. The fibres have an orientation of c-
427 axis parallel to morphological axis of crystals. The fibrous median lamina is forming
428 small fascicles of fibres, some with large morphologies, as in the middle region of the
429 image, and others with shorter irregular elongated morphologies in the upper region of
430 the image. Three main areas, as in the previous example, can be recognized in
431 orientation images (two microlamellar sclerenchyma and the median lamina) (Fig. 7e).
432 The two microlamellar walls are completely co-oriented in the azimuth of c-axis, but
433 they are misoriented in their inclination ~40° (Fig. 7f), depending on the distance to the
434 median lamina. The left wall shows an inclination of their c-axis of ~75-85°, whereas
435 the right wall has an inclination ~50-60° in the areas close to the median lamina and
436 ~35-40° in the areas close to the lumen. Moreover, the median lamina has two kinds of
437 orientations. The fibres close to the left side have an inclination of ~70-75° and
438 gradually changes to ~-30-40° in the centre of the median lamina. The right lamellar

sclerenchyma shows two maximal orientations (azimuth) of their c-axis, misoriented each other ~40° (Fig. 7f). This variation may be interpreted as the rotation around the corallite side and it can be observed in the micrograph (Fig. 7d).

FIGURE 8

The crystallographic arrangement of *Roemeria infundibulifera* was studied in a transverse (Fig. 8a-c) and an almost longitudinal sections (Fig. 8d-f). Petrographic micrographs of the sections of the corallites show that these skeletons are composed of alternating domains of lamellae and fibres separated by a median lamina composed of hyaline elements (Fig. 8a, d). Both, fibres and lamellae have a concordant and correlated c-axis orientation (azimuth) between two corallites (parallel and perpendicular to the morphological axis respectively) (Fig. 8b, e). The lamellar domain in the transverse section shows a broad distribution of their c-axis orientation (azimuth) ~45° due to the rotation of the wall around the corallite (Fig. 8b). The c-axis inclination in lamellae and fibres near to median lamina is ~30-35° (Fig. 8b-c) regarding their morphological axis, and is similar in the longitudinal section (Fig. 8e-f). The lamellar domains near to the lumen show an inclination of ~60° (Fig. 8b-c). The hyaline elements of the median lamina are disseminated in the middle of two walls and they do not form a continuous lamina (Fig. 8a, d). The representation of orientations of each crystal has been expressed in a pole figure (Fig. 8c), in which random orientations of their c-axis of different elements can be appreciated. On the other hand, the left part of the area studied in the longitudinal section shows a different pattern of orientation, which seems to proceed from the lumen of the corallite (Fig. 8e). This area shows a random orientation between the microstructural elements, probably due to a diagenetical alteration front from the lumen (Fig. 8f).

463 FIGURE 9

464 *Roemeripora bohemica* shows a high variation in the c-axis orientation of their
465 microstructure (Fig. 9a-b). The petrographic micrograph (Fig. 9a) shows two fibrous
466 and lamellar walls separated by a lamina media composed of hyaline elements with a
467 discontinuous appearance. The fibrous area is small compared with the lamellar domain
468 and it is near to the median lamina. The orientation (azimuth) of the c-axis of lamellae
469 and fibres is concordant in both walls (perpendicular and parallel to the morphological
470 axis, respectively) and the inclination is variable between both walls. The right wall
471 shows an inclination similar to that described in other taxa (~55-65°), whereas the left
472 wall shows an inclination between ~70-85°. The hyaline elements of the median lamina
473 have random orientations (Fig. 9c), mostly with a single orientation of each crystal. The
474 skeletons show clear evidences of diagenetical alteration in some areas that show
475 random orientations. On the other hand, the shared-wall of *Roemeria cubiniensis* shows
476 a microstructure composed of short irregular fibres disposed in rows (Fig. 9d) separated
477 by a median lamina of disseminated hyaline elements. The orientation is concordant
478 between two walls, being parallel to the morphological axis of the fibres and in this case
479 also to the rows. The inclination of microelements is variable between two walls,
480 depending on the corallite and the distance to the median lamina. The maximum pole is
481 focused in the lower side of the image at ~60-70° near to the lumen and at ~35-40° near
482 to the median lamina. Furthermore, the fibres of the upper wall of the image have a
483 maximum at ~35-40° in areas close to the median lamina and at ~5-10° near to the
484 lumen. On the other hand, the median lamina is composed of irregular microcrystals
485 (stelloid-shape) with a random c-axis orientation (Fig. 9f). The uppermost part of the
486 image shows a diagenetical alteration zone that has advanced to the median lamina from
487 the right part of the image.

Neomultithecopora cantabrica allows studying the in situ variation of c-axis orientation between phaceloid to pseudocerioid-ceriod internal structure. The samples studied by CIP correspond with two transverse sections of a cerioid (Fig. 10a-c) and phaceloid growth (Fig. 10d-e). The petrographic micrograph (Fig.10a) shows a cerioid transverse section with two lamellar sclerenchyma separated by an irregular (slightly wavy) granular median lamina (Fig. 10a). The lamellar domains show a concordance c-axis orientation (azimuth) in the lamellae (perpendicular to the morphological axis) and the variation of inclination in both walls is similar ~25-35° (Fig. 10c). The granular zone has many regions with variable c-axis orientations with diverse colourations (Fig. 10b), a similar pattern has been observed in the lower wall and some scattered zones in both walls. These regions have random c-axis orientation patterns (Fig. 10c), which indicates diagenetical alteration. Nonetheless, the granules of median lamina still show original orientations with concordant directions to the main microstructural elements. The inclination in those zones are high, with values ~75-85°, as shown by the light colourations in these regions. The phaceloid section of *N. cantabrica* is composed of an inner fibrous domain in the palisade and an external lamellar domain (Fig. 10d). This main lamellar domain has a c-axis orientation (azimuth) perpendicular to the morphological axis and toward the lumen (Fig. 10e-f) and an inclination of ~20-35° depending on the location in the section (Fig. 10f). The fibrous domain and some areas of the lamellar domains have random c-axis orientation, specifically the areas in contact with the lumen, although some fibres still show original (azimuth and inclination) c-axis orientation (Fig. 10e). The same process occurs with the lamellae in contact with the matrix.

FIGURE 10

512 A halysitid shared-wall between two corallites over a connecting tubule has been
513 studied in *Pleurosiphonella* sp. (Fig. 11a-c). The orientation image shows a complex
514 conformation of the shared wall. The microstructure of *Pleurosiphonella* sp. is
515 composed of a main lamellar domain and external inner fibrous domain. The main
516 orientations are subdivided by quadrants separated by a symmetric plane along the
517 connecting tubule and a net contact between corallites, as explained above. In those
518 areas close to the contact between walls, the microelements are small, they have
519 irregular morphologies (Fig. 11a) and their orientations depend on their position in the
520 wall. The flattened microstructure close to the contact area is conditioned by the
521 stretching of corallites. The c-axis orientation (azimuth) of the structure can be
522 subdivided in three main orientations (Fig. 11b-c), cool colourations in the pole figure
523 (blue and purple). The symmetric plane separate two areas (upper and lower in the
524 image) misoriented ~40° in both walls. In turn, the left wall exhibits a gradual change in
525 the disposition of its microstructure (upper left part of image), recovering the cylindrical
526 conformation of the skeleton, misorienting the connecting area and the cylindrical
527 sclerenchyma ~60°. The main inclination of the c-axis in the different quadrants of
528 connecting structure is ~15º, whereas in the cylindrical conformation is ~30-35° and in
529 the lower quadrant of right wall is ~60°. On the other hand, a phaceloid transverse
530 section of *Pleurosiphonella* sp. (Fig. 11d-f) shows alternating lamellar and fibrous
531 domains (F-L-F). Both lamellae and fibres show a c-axis orientation coherent with the
532 previous results. The transverse section shows a continuous orientation except for some
533 small areas with visible diagenetical alteration, which exhibit a different orientation and
534 are close to the matrix and lumen areas. The maximum pole (inclination) is focused
535 ~30° with some variations of 15-60° in some points of the section. The orientation
536 (azimuth) is variable ~40°, similar to other taxa studied (Fig. 11f).

The correlated misorientation has been calculated by punctual measurement between two crystals (200 points per image). The CIP method has crystallographic sensitivity greater than 10° (Trimby & Prior 1999), although we have measures some small variations above 5°, the differentiation between crystals with the same orientation or a variation less than 5° is difficult with this methodology and for this reason the results may be somewhat different to EBSD analysis, in which the main order of misorientation for Syringoporicae is 5° (Coronado *et al*., 2014b). Similar results of the main misorientation obtained here were shown by Coronado *et al*. (2014a) in *Sinopora*. The misorientation results for all studied taxa have been summarized in histograms in Figure 12. The trend of misorientation depends on the analysed sections (oblique or transverse) and their internal structural organization (phaceloid or cerioid). There is a common result in all taxa independently of their internal structural organization. The main misorientation is 10° together with 5° in some phaceloid corals (green graphs). The general trend in the cerioid corals (blue graphs) is a lognormal distribution with a gradual decrease of the misorientation to higher angles (e.g. *Roemeripora*, *Roemeria bohemica*, *R. infundibulifera* and *Neomultithecopora cantabrica*), variations in the trend can be related with the studied sections (transverse, or slightly oblique or the presence of wall elements). Similar results were obtained with EBSD for *Roemeripora* sp. in which the difference of 5° was the main order of misorientation. Otherwise, the phaceloid taxa show a lognormal distribution with an abrupt decrease from the main misorientation (interval to 5-10°) to higher angles. The example of *Neomultithecopora cantabrica* is the most representative (Fig. 12h-i) with diverse trends in the different internal structural organization. *Pleurosiphonella* sp. shows that depending on the section, the misorientation values vary. Figure 12e shows the values of misorientation

561 of the shared-wall example in the connecting tubuli versus the cylindrical section (Fig.
562 12f).

563 FIGURE 11

564 **5. Discussion**

565 **5. a. Micro- and nanostructure: a result of matrix-mediated biomineralization**

566 The data described here reveal that the crystallo-structural properties of Syringoporicae
567 have still preserved most of their biogenic properties. The microstructural and
568 nanostructural characteristics of the studied Syringoporicae are common in all of the
569 taxa despite their internal structural organization and their differences in the
570 crystallographic arrangement. Following the criteria proposed by Mann (2001) it can be
571 inferred that the Syringoporicae skeletons are composed of hierarchical structures from
572 mm to nm scale. The skeletons are composed of "*well defined structures*" as a calcitic
573 sclerenchyma composed by concentric microdomains, septal spines and tabules. The
574 variation in the size, morphology and distribution of micro-domains reveals that these
575 features are conditioned by the taxonomy (Table, 1), showing distinctive "*uniform*
576 *particle sizes"* for each taxon. An example of this can be seen in Figure 13 where the
577 different sizes (length and width) of nanocrystals have been plotted for each taxon
578 taking into account their morphologies. The box charts reveal that the nanostructure of
579 *Neomultithecopora cantabrica* is similar between the samples of the two different
580 localities. The modest differences appear to be related with the intraspecific variation,
581 but the morphology, the median values and their distribution is similar between them.
582 Conspicuous differences can be observed between other taxa, highlighting that those
583 with similarities in size have different morphologies. Both at microscale as nanoscale
584 the units that form the different bricks have "*high levels of spatial organization*". On the

585 one hand, imbricate calcite crystals (fibres and lamellae) forming either micro-domains
586 or wall elements are observed at microscale. On the other hand, at nanoscale the
587 microcrystals are composed of nanounits that form nanolaminae arranged in
588 submicrometric intralaminations. Both micro- and nanounits have "*complex*
589 *morphologies*" composed of curved crystals very different to their inorganic
590 counterparts. The alternating domains reveal at microscale a "*controlled aggregation*
591 *and texture*" by the control produced by epithelial cells, which are responsible for
592 mineralization in some Anthozoa (e.g. Scleractinia), and this control can be seen at
593 nanoscale where the co-oriented nanocrystals show that each microcrystal is forming a
594 bio-composite (Mann, 2001). The gradual transition between lamellae, fibres and
595 equidimensional granules with intermediate morphologies is a common characteristic
596 between all taxa and it seems to be an essential property in Palaeozoic corals
597 (Semenoff-Tian-Chansky, 1974; Lafuste, 1978, 1983; Rodríguez, 1989, Falces &
598 Rodríguez, 1999). As explained above, both micro- and nanotextures have a
599 "*preferential crystallographic orientation*", which suggest a great crystallographic
600 control exerted by the epithelial tissue as was shown also in previous studies of other
601 taxa of this superfamily (Coronado *et al*., 2013; 2014a,b). This fact suggests that the
602 epithelial cells are almost in contact with the mineralized substrate. All these evidences
603 emphasize that the Syringoporicae skeletons are composed of highly organized "*self-*
604 *assembled structures,*" as was shown by Coronado *et al*. (2013) for *Multithecopora*
605 *hontoriense*.

606 FIGURE 12

607 The new data presented here support that the Syringoporicae skeletons are a product of
608 matrix-mediated biocrystallization. This hypothesis was established by Coronado *et al*
609 (2014b) from crystallographic evidences, stating that skeletons are formed by a co-

610 ordinated stepping growth mode. In the first place, the dark envelope observed around
611 nanocrystals in all of the samples studied, which are thicker between nanolaminae, have
612 been interpreted by previous authors as intracrystalline organic matrix (Dauphin, 2002;
613 Rousseau *et al*., 2005; Cuif *et al*., 2008; Baronnet *et al*., 2008; Checa *et al*., 2013;
614 Gorzelak *et al*., 2013). This organic matrix could correspond with an organic-hydrogel
615 secreted by epithelial cells. This model supports the idea that the growth would be
616 produced at steps, from the secretion of the organic matrix, which acted as a site of
617 crystallization. The process of biocrystallization continues by addition of organic layers
618 and their subsequent crystallization, forming submicrometric intralamination to form
619 the microcrystal. This process has been described and coined by Cuif *et al*. (2012) for
620 scleractinian and molluscs, from the observation of these organic phases by AFM and
621 their confirmation by structural and compositional evidences. Also, it has been
622 suggested for other groups where this kind of evidences (organic linings and
623 intralamination) can be observed in both structural and compositional level, as
624 echinoderms, foraminifers and brachiopods (Cusack *et al*., 2008; Cuif *et al*., 2012,
625 2013; Gorzelak *et al*., 2013). Although this model only can clarify the formation of
626 single microcrystals, it is necessary to understand the process of formation of a
627 complete framework and the relations between the microunits. In this point, Coronado
628 *et al*. (2014b) interpreted on the basis of crystallographic data that the nucleation
629 between co-oriented crystals could be produced by a mechanism similar to mineral
630 bridges, maintaining the preferred crystallographic orientations during the process of
631 growth. The misorientation study revealed that most part of microcrystals are co-
632 oriented and the EBSD images showed that they are separated by a dashed line, which
633 was attributed to intercrystalline organic matrix, whereas the misoriented crystals have a
634 most continuous intercrystalline organic matrix. The new data of AFM contributed here

635 to support this hypothesis. The contact between co-oriented microcrystals is bridged by
636 co-oriented nano-units and the etched valley between crystals is deeper and continuous
637 between those misoriented microcrystals. Thus, during the secretion of organic-
638 hydrogel two kinds of organic matrices are differentiated. The porous intercrystalline
639 organic matrix, which could be responsible for acting as template for the morphology of
640 microcyrstals confining the biocrystallization, and the intracrystalline organic matrix
641 could be responsible of growth of the nano-units and their posterior conformation in
642 microcrystals by aggregation of nanolaminae.

643 Thus, the skeleton structure (at micro- and nanoscale) seems to be a reflection of the
644 genetic code. The modes of growth and conformation of microstructures are
645 homogeneous in all studied taxa and comparable with previous studies (Coronado *et al*.,
646 2013, Coronado *et al*. 2014a, b). Likewise, the variation in sizes and morphologies of
647 micro- and nanocrystals seem to be related with taxonomy.

648 FIGURE 13

649 **5. b. Shared-walls: meaning of median lamina**

650 As described above, three principal kinds of calcite crystals are recognized in the
651 studied taxa: lamellae, fibres and granules (equidimensional and hyaline elements).
652 Regardless of the morphology of the crystals, the fibres and lamellae in the different
653 taxa have common crystallographic characteristics, with the c-axis oriented (azimuth)
654 toward the lumen. The inclination is variable and depends on the internal structural
655 organization. The phaceloid taxa (*Neomultithecopora cantabrica* and *Pleurosiphonella*
656 sp.) have a distinctive inclination of c-axis of 20-35° with respect to the microcrystal.
657 An equivalent value was measured by EBSD and CIP in other phaceloid Syringoporicae
658 (Coronado *et al*., 2014a, b). This value seems to represent the inclination of the lamellae

659 with respect to the growth direction (according to the morphological axis). This value is
660 variable in the cerioid / pseudocerioid taxa. Some cerioid taxa show an inner variation
661 of c-axis inclination along the wall excluding the median lamina. This variation
662 corresponds with a misorientation between the areas (external to internal) of ~30° and
663 usually the higher inclination is located toward the lumen, may be conditioned by the
664 presence of wall structures as septal spines or tabules and it depends on the inclination
665 of these structures respect to the lumen [as occur in *Roemeria infundibulifera*, *R.*
666 *cubiniensis* and *Roemeripora* sp.; details of wall elements in Lafuste & Tourneur,
667 1988a; Coronado *et al*., 2014b)]. Coronado *et al*. (2014b) showed that the formation of
668 these wall elements conditioned the surrounding microstructure and their
669 crystallographic arrangement. Even so, the most common value in the transverse section
670 for the inclination of c-axis of microelements is ~30-35°, similar to phaceloid taxa.
671 Some shared-walls have a variation of c-axis inclination between them. *Roemeripora*
672 sp. (in the transverse section) and *Roemeria bohemica* show misoriented c-axis
673 inclination in shared-walls ~40 and 20° respectively. Petrographic micrograph of
674 *Roemeripora* sp. in Coronado *et al*. (2014b) showed that the interference colour under
675 polarized light never match with the median lamina in any side of the prismatic wall but
676 in some sides the colour (which indicate c-axis orientation) is similar between two
677 shared-walls, coinciding with the observations with CIP in the most of the studied taxa.
678 This complex conformation can be related with the origin of the median lamina.

679 The crystallographic and structural data have revealed two singular features about the
680 hyaline elements. One of them is that they never have gradual transit to other
681 sclerenchyma microelements, as happens in the transit of fibres, lamellae and
682 equidimensional granules. Besides, the crystallographic orientations (azimuth) of c-axis
683 of hyaline element, independently of their morphology, always have a random

684 orientation in regard to the sclerenchyma. These two features seem to indicate that the
685 hyaline elements have an inorganic origin. As Lafuste & Tourneur (1991) described in
686 *Thamnopora* and can be seen in the Syringoporicae studied here, the hyaline elements
687 show the presence of spotted opaque particles in the interior of some crystals observed
688 by petrographic microscopy, suggesting that these spots are remains of organic matter
689 preserved within the crystals. This could explain the presence of hyaline elements and
690 the interruption of growth between both corals. The median lamina with hyaline
691 elements is discontinuous and the hyaline elements could be spaces where the epithelial
692 tissue was trapped between two shared-walls during growth. After the organic decay,
693 the biomolecules were occluded by the crystals faces as inclusions during the
694 precipitation of cements into spaces. The crystallization in presence of organic
695 compounds can generate irregular morphologies that could have suggested to Lafuste &
696 Tourneur (1991) the organic origin of these structures. Recently, there are numerous
697 experiments of controlled crystallization in presence of organic molecules and their
698 control over morphological habits, which change substantially (Falini *et al*., 2007;
699 Goffredo *et al*., 2011; Nindiyasari *et al*., 2014 a). These evidences suggest that hyaline
700 elements should be not considered as granules.

701 FIGURE 14

702 A singular feature of the median lamina composed of equidimensional granules is the
703 presence of a high inclination of c-axis. *Roemeripora* sp. and *Neomultithecopora*
704 *cantabrica* median laminae show, by the c-axis orientations (azimuth), that both walls
705 take part in the growth of this lamina. The variation of inclination between the walls and
706 the granules of median lamina is ~20-50°. There are some evidences in the studied taxa
707 that help to understand the origin of granules. One of them is found in *Pleurosiphonella*
708 sp. where the microelements of the connecting tubule change their morphologies in the

709 contact zone where the crystal size is reduced. The inclination of c-axis in these areas is
710 varied, losing the regular inclination ~30° for ~15°, which indicate a stretching of
711 polyps during the growth. Even so, the connecting tubule is growing forming a
712 cylindrical structure as the misorientation study shows (Fig. 12f). In the case of
713 *Roemeripora* sp. or *N. cantabrica* the microelements near the median lamina change
714 their morphology, passing to intermediate morphologies (cupolar-shape to granules in
715 *Roemeripora* sp. or irregular fibres to granules in *N. cantabrica*). Apart from this
716 evidence, in the case of *Roemeripora* sp., a process of 'fibrization' of the median lamina
717 (Lafuste *et al*., 1992) can be observed in thickened areas, in which the median lamina is
718 composed of fibres. This process has been described in other Palaeozoic corals
719 (Tourneur, 1987; Lafuste & Tourner, 1988b; Lafuste *et al*., 1992). An orientation image
720 of this area reveals that the fibres of the median lamina have an inclination of the c-axis
721 that depends on the inclination of both sides, in this case the left wall has an inclination
722 of ~75-85° and the fibres have an inclination ~75°, whereas in the right side the fibres
723 are at ~40° and the microlamellae of right side at ~50-60°. This fact suggests that during
724 the growth process due to the proximal contact of polyps in a cerioid structure the
725 epithelial tissues of two polyps were in contact during the secretion (as occurs in
726 *Pleurosiphonella* sp.). Coronado *et al*. (2014b) interpret that the secretion begins in the
727 external part of the corallite towards the lumen. As explained above, the biomineral
728 features of Syringoporicae reveal that the epithelial cells were very close to the skeleton,
729 controlling the biocrystallization process almost in contact. Thus, variation in the
730 position of epithelial tissue (either stretching or folding) varies the space of
731 crystallization and their crystallographic properties and morphology of microcrystals.
732 Consequently, the high c-axis inclinations of granules indicate that the two epithelial
733 tissues are in contact and probably folded up. In that situation, the growth of

734 microelements (e.g. fibres) is aborted and the equidimensional granules are formed due
735 to lack of space between both walls. An example of this can be observed in Figure 4e,
736 where the fibres of *Neomultithecopora cantabrica* began to grow, but they are aborted,
737 appearing as granules. During the vertical development of the colony, the polyps grow
738 and the diameter of corallites is widened and the wall is thickened whereby there is
739 more space to secrete a true domain of fibres. These have a concordant inclination in
740 regard to the walls that belong, as occurs in *Roemeripora* sp. The equidimensional
741 granules have been described in the middle of septa, basal surfaces of tabulae and
742 dissepiments, and in shared-walls of colonial forms in rugose and tabulate corals. All
743 these locations are related to reduced space for growth of microelements.

744 **5. c. Cerioid growth: a genetic architectonical solution**

745 Mann (2001) stated that the main control mechanisms in biomineralization processes
746 are governed by a gene pool, which is conditioned by bioenergetic processes (e.g.
747 growth of corals during the day in the presence of the sun or by the presence of
748 nutrients) and adapted to environmental influences. These control mechanisms are a
749 complex interrelated network and they are chemical (ion transport, saturation), spatial
750 (confining processes of supramolecular organization), structural (preferential
751 nucleation), morphological (morphogenesis) and constructional (higher-order
752 structures). The biomineralization process in Syringoporicae is controlled mainly from
753 molecular level to mm scale by the genetic code, as was displayed before.

754 FIGURE 15

755 The variation in the astogeny (pattern formation in colonial organisms, Hammer, 1998)
756 is common in the Syringoporicae as an architectonical solution to environmental
757 fluctuations stabilising the colony. Different strategies have been described; as

758 prostrated and reticulated growth (e.g. ‘auloporoid reticulum’ in *Multithecopora*,
759 Tchudinova, 1986), erect corallum with reticulated connecting structures (e.g.
760 *Syringopora*, Nowinski, 1991), cerioid massive dome-shaped corallum (e.g. *Roemeria*,
761 Mistiaen, 1988) or irregular cateniform palisades of halysitid corals (e.g. *Catenipora*,
762 Hammer, 1998). These changes have also been interpreted as improved feeding system
763 (Hammer, 1998, cites herein). The intraspecific variation of internal structural
764 organization or astogenetic changes of Syringoporicae (phaceloid or cerioid) depends on
765 spatial, structural and morphological controls. As an example, in colonies of
766 *Neomultithecopora cantabrica* and *Roemeria*, the internal structure of the corallum
767 changes from phaceloid to cerioid when subjected to the waves action (Fig. 15). On the
768 contrary, other Syringoporicae subjected to environmental stress conditions (increasing
769 wave energy), arrange the corallites and their morphologies in irregular patterns without
770 losing the phaceloid arrangement (Coronado & Rodríguez, 2014). The crystallographic
771 data provided here suggest that in spite of the environmental conditions the
772 crystallographic arrangement and the final morphology of corallum are only controlled
773 by the genetic code. The cerioid taxa have specific misorientation and c-axis inclination
774 variation which can be conditioned by the disposition of the microcrystals in individual
775 sides in a prismatic structure (Fig. 15) instead of correlative variation in a cylindrical
776 structure (Fig. 15).

777 The ability of some families of Syringoporicae to arrange the microstructures in other
778 system may be a potential adaptive advantage to colonize other environments. This
779 could be explained by the development of a structure that remains as a honey-comb in
780 cerioid coralla. These structures are known as ‘cellular structures’ (Gibson & Ashby,
781 1997), which are an interconnected network of solid pillars or plates which form the
782 edges and faces of cells are very common in the natural world (as woods, bones, sponge

783 structures). Some of the most important features of a cellular solid are its relatively low
784 density and its high plasticity under uniaxial and biaxial deformations (Gibson &
785 Ashby, 1997). Under seawater, the maximum efforts are conditioned by wave energy,
786 which could produce uniaxial deformation of the colonies in conditions of maximum
787 stress and the pores of connection between corallites could favour this mechanism,
788 allowing the passage of water. This feature together with the prismatic morphology of
789 corallites at macroscale is a relevant strategy to avoid fracture by cleavage; because the
790 main orientation of the c-axis in each side of wall is misoriented 60° (Fig. 15), it could
791 have been an evolutionary advantage to colonize marine realms during the Palaeozoic.

792 **6. Conclusions**

793 The structural and crystallographic comparative study of cerioid, pseudoceriod and
794 phaceloid taxa with shared-walls have revealed:

795 - Micro- and nanotextural features are common in all of skeletons studied,
796 showing that they were composed of hierarchical structures from mm to nm.
797 - The data presented here show that the Syringoporicae skeletons are a product of
798 matrix-mediated biocrystallization, suggesting a co-ordinated stepping growth
799 mode for the formation of microcrystals and a growth system similar to mineral
800 bridges to produce the whole skeleton. Thus, the data reveal that the skeleton
801 structure is a reflection of the genetic code.
802 - The median lamina is formed by the joint crystallization of both polyps at the
803 same time. Crystallographic data reveals that the hyaline elements have an
804 inorganic origin, in contrast to equidimensional granules. The crystallographic
805 and structural data reveal that the granules could be aborted fibres during the
806 growth of two corallites in contact.

- The variation in the internal structural organization (phaceloid, or cerioid) is conditioned by the environment but the final structure is controlled by genetic. The modifications are observable in the crystallographic arrangement, which is controlled by genetics, which is derived from the disposition of epithelial tissue.

Acknowledgements

Financial support through the Spanish Ministerio de Economía y Competitividad (research project CGL2012-30922BTE) and Complutense University Research Group (910231) is gratefully acknowledged. Ismael Coronado acknowledges financial support through a FPI-UCM grant and a Synthesis grant (FR-TAF-2397) developed in MNHN (Paris, France) during 2012, which allowed studying the material of Lafuste's collection. We sincerely thank the staff of the Centro Nacional de Microscopía Electrónica (CNME, Complutense University of Madrid, Spain), where was used the SEM and AFM. This research is a contribution to the IGCP Project 596 (Climate change and biodiversity patterns in the Mid-Palaeozoic). We also give our sincere thanks to Ian D. Somerville (UCD) for his advice and the English revision of the manuscript.

Declaration of Interest

The authors declare no competing financial interests.

References

BALTHASAR, U., CUSACK, M., FARYMA, L., CHUNG, P., HOLMER, L. E., JIN, J., PERCIVAL, I. G. & POPOV, L. E. 2011. Relic aragonite from Ordovician–Silurian brachiopods: Implications for the evolution of calcification. *Geology* 39(10), 967-70.

BARBIN, V., RAMSEYER, K. & ELFMAN, M. 2008. Biological record of added manganese in seawater: a new efficient tool to mark in vivo growth lines in the oyster species *Crassostrea gigas*. *International Journal of Earth Sciences* 97(1), 193-99.

BARONNET, A., CUIF, J. P., DAUPHIN, Y., FARRE, B. & NOUET, J. 2008. Crystallization of biogenic Ca-carbonate within organo-mineral micro-domains. Structure of the calcite prisms of the Pelecypod *Pinctada margaritifera* (Mollusca) at the submicron to nanometre ranges. *Mineralogical Magazine* 72(2), 617-26.

BARRET, S. 1997. Image analysis and the internet *Scientific Data Management* 1, 18-25.

BENZERARA, K., MENGUY, N., OBST, M., STOLARSKI, J., MAZUR, M., TYÑISCZAK, T., BROWN JR., G. E. & MEIBOM, A. 2011. Study of the crystallographic architecture of corals at the nanoscale by scanning transmission X-ray microscopy and transmission electron microscopy. *Ultramicroscopy*.

BERMAN, A. 2010. Biomineralization of Calcium Carbonate. The Interplay with Biosubstrates. In *Biomineralization* pp. 167-205. John Wiley & Sons, Ltd.

BROOD, K. 1978. Skeletal structures of Silurian auloporid corals. *Geologiska Föreningen i Stockholm Förhandlingar* 100(1), 53-63.

CORONADO, I. & RODRÍGUEZ, S. 2014. Carboniferous auloporids from the Iberian Peninsula: palaeocology, diversity, and spatio-temporal distribution. *Journal of Iberian Geology* 40(1), 61-85.

CORONADO, I., PÉREZ-HUERTA, A. & RODRÍGUEZ, S. 2013. Primary biogenic skeletal structures in *Multithecopora* (Tabulata, Pennsylvanian). *Palaeogeography, Palaeoclimatology, Palaeoecology* 386(0), 286-99.

CORONADO, I., PÉREZ-HUERTA, A. & RODRÍGUEZ, S. 2014a. Computer-integrated polarisation (CIP) in the analysis of fossils: a case of study in a Palaeozoic coral (*Sinopora*, Syringoporicae, Carboniferous). *Historical Biology*, 1-15.

854 CORONADO, I., PÉREZ-HUERTA, A. & RODRÍGUEZ, S. 2014b. Crystallographic
855 orientations of structural elements in skeletons of Syringoporicae (tabulate corals,
856 Carboniferous): implications for biomineralization processes in Palaeozoic corals.
857 *Palaeontology*, n/a-n/a.
858 CUIF, J. P., DAUPHIN, Y. & GAUTRET, P. 1999. Compositional diversity of soluble
859 mineralizing matrices in some recent coral skeletons compared to fine-scale growth
860 structures of fibres: discussion of consequences for biomineralization and diagenesis.
861 *International Journal of Earth Sciences* 88(3), 582-92.
862 CUIF, J. P., DAUPHIN, Y., FARRE, B., NEHRKE, G., NOUET, J. & SALOMÉ, M. 2008.
863 Distribution of sulphated polysaccharides within calcareous biominerals suggests a
864 widely shared two-step crystallization process for the microstructural growth units.
865 *Mineralogical Magazine* 72(1), 233-37.
866 CUIF, J.-P., DAUPHIN, Y. & SORAUF, J. E. 2011. *Biominerals and fossils through time*.
867 Cambridge; New York: Cambridge University Press.
868 CUIF, J.-P., DAUPHIN, Y., NEHRKE, G., NOUET, J. & PEREZ-HUERTA, A. 2012. Layered
869 Growth and Crystallization in Calcareous Biominerals: Impact of Structural and
870 Chemical Evidence on Two Major Concepts in Invertebrate Biomineralization Studies.
871 *Minerals* 2(1), 11-39.
872 CUSACK, M., DAUPHIN, Y., CUIF, J.-P., SALOMÉ, M., FREER, A. & YIN, H. 2008b.
873 Micro-XANES mapping of sulphur and its association with magnesium and phosphorus
874 in the shell of the brachiopod, *Terebratulina retusa*. *Chemical Geology* 253(3–4), 172-
875 79.
876 CUSACK, M., DAUPHIN, Y., CHUNG, P., PÉREZ-HUERTA, A. & CUIF, J. P. 2008a.
877 Multiscale structure of calcite fibres of the shell of the brachiopod *Terebratulina retusa*.
878 *Journal of Structural Biology* 164(1), 96-100.

879 CHECA, A. G., MUTVEI, H., OSUNA-MASCARÓ, A. J., BONARSKI, J. T., FARYNA, M.,
880 BERENT, K., PINA, C. M., ROUSSEAU, M. & MACÍAS-SÁNCHEZ, E. 2013.
881 Crystallographic control on the substructure of nacre tablets. *Journal of Structural*
882 *Biology* 183(3), 368-76.
883 DAUPHIN, Y. 2002. Fossil organic matrices of the Callovian aragonitic ammonites from
884 Lukow (Poland): location and composition. *International Journal of Earth Sciences*
885 91(6), 1071-80.
886 FALCES, S. & RODRÍGUEZ, S. 1999. Observations on the skeletogenesis of rugose corals.
887 In *Abstracts of the 8th International Symposium on Fossil Cnidaria and Porifera* p. 44.
888 FALINI, G., MANARA, S., FERMANI, S., ROVERI, N., GOISIS, M., MANGANELLI, G. &
889 CASSAR, L. 2007. Polymeric admixtures effects on calcium carbonate crystallization:
890 relevance to cement industries and biomineralization. *CrystEngComm* 9(12), 1162-70.
891 FRYDA, J., KLICNAROVA, K., FRYDOVA, B. & MERGL, M. 2010. Variability in the
892 crystallographic texture of bivalve nacre. *Bulletin of Geosciences* 85(4), 645-62.
893 GAUTRET, P. 2000. Matrices organiques intrasquelettiques des scléractiniaires récifaux:
894 Évolution diagénétique précoce de leurs caractéristiques biochimiques et conséquences
895 pour les processus de cimentation. *Geobios* 33(1), 73-78.
896 GIBSON, L. J. & ASHBY, M. F. 1997. *Cellular solids : structure and properties*.
897 Cambridge University Press.

898 GOFFREDO, S., VERGNI, P., REGGI, M., CAROSELLI, E., SPARLA, F., LEVY, O.,
899 DUBINSKY, Z. & FALINI, G. 2011. The Skeletal Organic Matrix from Mediterranean
900 Coral *Balanophyllia europaea* Influences Calcium Carbonate Precipitation. *Plos One*
901 6(7).
902 GORZELAK, P., STOLARSKI, J., MAZUR, M. & MEIBOM, A. 2013. Micro- to nanostructure
903 and geochemistry of extant crinoidal echinoderm skeletons. *Geobiology* 11(1), 29-43.

HAMMER, O. 1998. Regulation of astogeny in halysitid tabulates. *Acta Palaeontologica Polonica* 43(4), 635-51.

HEILBRONNER, R. & BARRET, S. 2014. *Image Analysis in Earth Sciences - Microstructures and Textures of Earth Materials*. London: Springer.

HEILBRONNER, R. 2000. Automatic grain boundary detection and grain size analysis using polarization micrographs or orientation images. *Journal of Structural Geology* 22(7), 969-81.

HEILBRONNER, R. P. & PAULI, C. 1993. Integrated spatial and orientation analysis of quartz c-axes by computer-aided microscopy. *Journal of Structural Geology* 15(3–5), 369-82.

HILL, D. 1981. Rugosa and Tabulata. *Teichert C. (ed.). Treatise on Invertebrate Paleontology, Part F [Coelenterata] Suppl. 1, Boulder/Colorado & Lawrence/Kansas*, 672.

HORCAS, I., FERNÁNDEZ, R., GÓMEZ-RODRÍGUEZ, J. M., COLCHERO, J., GÓMEZ-HERRERO, J. & BARO, A. 2007. WSXM: a software for scanning probe microscopy and a tool for nanotechnology. *Review of Scientific Instruments* 78(1), 8.

LAFUSTE, J. & PLUSQUELLEC, Y. 1986. Les caulicules, éléments nouveaux de l'axe des trabécules du Tabulé dévonien *Ligulodictyum* Plusquellec 1973. *Comptes rendus de l'Académie des sciences. Série 2, Mécanique, Physique, Chimie, Sciences de l'univers, Sciences de la Terre* 303(8), 761-64.

LAFUSTE, J. & PLUSQUELLEC, Y. 1988. Révision des *Beaumontia* décrits par Milne-Edwards et Haime (Tabulata ; Dévonien, Carbonifère). *Bulletin du Museum National d'Histoire Naturelle. Paris, 4ª série* 10. C(3), 179-97.

927 LAFUSTE, J. & PLUSQUELLEC, Y. 1990. Les genres *Utaratuia*, *Tabellaephyllum*,
928 *Michelinia* et la distinction Tabulata-Rugosa. *Annales de Paléontologie (Vert.-Invert.)*
929 76(1), 13-39.
930 LAFUSTE, J. & TOURNEUR, F. 1988a. Précisions sur la structure et la microstructure du
931 genre *Roemeria* Milne-Edwards & Haime 1851 (Tabulata, Dévonien moyen
932 d'Allemagne et de Belgique). *Paläontologische Zeitschrift* 62(1-2), 11-48.
933 LAFUSTE, J. & TOURNEUR, F. 1988b. *Dendropora* Michelin, 1846, et le nouveau genre
934 dendroporimorphe *Senceliaepora* du Givétien et du Frasnien de la Belgique et du
935 Boulonnais (France). *Bulletin du Museum National d'Histoire Naturelle. Section C,*
936 *Sciences de la terre, paléontologie, géologie, minéralogie* 10(4), 307-41.
937 LAFUSTE, J. & TOURNEUR, F. 1990. Structure et microstructure du genre *Kiaerites*
938 Stasińska, 1967 (Tabulata, Silurien de Norvège). *Geobios* 23(6), 655-69.
939 LAFUSTE, J. & TOURNEUR, F. 1991. Biocristaux et éléments foncés de la muraille chez
940 *Thamnopora* Steininger, 1831 (Tabulata, Dévonien). *Annales de Paléontologie* 77, 3-
941 20.
942 LAFUSTE, J. 1970. Lames ultra-minces a faces polies. Procede et applicationa la
943 microstructure des Madreporaires fossiles. *Comptes rendus hebdomadaires des seances*
944 *de l'Academie des Sciences Paris* 270, 679-81.
945 LAFUSTE, J. 1978. Modalites de passage des lamelles aux fibres dans la muraillede
946 Tabules (Micheliniidae) du Devonien et du Permien. *Geobios* 11(3), 405-08.
947 LAFUSTE, J. 1981. Structure et microstructure de *Dendropora* Michelin 1846 (Tabulata,
948 Devonien). *Bulletin de la Societe Geologique de France* 23(3), 271-77.
949 LAFUSTE, J. 1983. Passage des microlamelles aux fibres dans le squelette d'un Tabulé
950 "michelinimorphe" du Viséen du Sahara algérien. *Geobios* 16(6), 755-61.

LAFUSTE, J., FERNÁNDEZ-MARTÍNEZ, E. & TOURNEUR, F. 1992. *Parastriatopora* (Tabulata) de las Calizas del Lorito (Devónico Inferior, provincia de Córdoba). *Revista Española de Paleontología* 7(1), 3-12.

LEE, M. R., TORNEY, C. & OWEN, A. W. 2012. Biomineralisation in the Palaeozoic oceans: Evidence for simultaneous crystallisation of high and low magnesium calcite by phacopine trilobites. *Chemical Geology* 314–317(0), 33-44.

LOWENSTAM, H. & WEINER, S. 1989. *On biomineralization*. New York: Oxford University Press.

MANN, S. 2001. *Biomineralization: Principles and concepts in bioinorganic materials chemistry*. Oxford: Oxford University Press.

MARIN, F., LE ROY, N., MARIE, B., RAMOS-SILVA, P., BUNDELEVA, I., GUICHARD, N. & IMMEL, F. 2014. Metazoan calcium carbonate biomineralizations: macroevolutionary trends – challenges for the coming decade. *Bulletin de la Societe Geologique de France* 185(4), 217-32.

MISTIAEN, B. 1988. Tabulés Auloporida du Givetien et du Frasnien de Ferques (Boulonnais - France). In *Le Dévonien de Ferques. Bas-Boulonnais (N. France)* (ed D. Brice). pp. 197-230. France.

MORENO-AZANZA, M., MARIANI, E., BAULUZ, B. & CANUDO, J. I. 2013. Growth mechanisms in dinosaur eggshells: an insight from electron backscatter diffraction. *Journal of Vertebrate Paleontology* 33(1), 121-30.

NICHOLSON, H. A. 1879. *On the structureand affinities of the Tabulate corals of the Palaeozoic period, with criticald escriptions of illustrative species*.

NINDIYASARI, F., FERNÁNDEZ-DÍAZ, L., GRIESSHABER, E., ASTILLEROS, J. M., SÁNCHEZ-PASTOR, N. & SCHMAHL, W. W. 2014. Influence of Gelatin Hydrogel Porosity on the Crystallization of CaCO3. *Crystal Growth & Design* 14(4), 1531-42.

NOWINSKI, A. 1991. Late Carboniferous to Early Permian Tabulata from Spitsbergen. *Palaeontologia Polonica* 51, 3-74.

OGILVIE, M. M. 1895. Microscopic and Systematic Study of Madreporarian Types of Corals. [Abstract]. *Proceedings of the Royal Society of London* 59, 9-18.

PEREZ-HUERTA, A. & CUSACK, M. 2008. Common crystal nucleation mechanism in shell formation of two morphologically distinct calcite brachiopods. *Zoology (Jena)* 111(1), 9-15.

PÉREZ-HUERTA, A., CUSACK, M. & ENGLAND, J. 2007. Crystallography and diagenesis in fossil Craniid brachiopods. *Palaeontology* 50(4), 757-63.

PÉREZ-HUERTA, A., CUSACK, M. & MÉNDEZ, C. A. 2012. Preliminary assessment of the use of electron backscatter diffraction (EBSD) in conodonts. *Lethaia* 45(2), 253-58.

PLUSQUELLEC, Y. & TCHUDINOVA, I. I. 1977. The microstrucuture of *Parastriatopora* Sokolov, 1949 (Siluro-Devonian Tabulata). *Annales de la Société géologique du nord* 97, 127-30.

PLUSQUELLEC, Y. 1976. Les polypiers. Tabulata.Les Schistes et Calcaires de l´Armorique (Dévonien inférieur, Massif Armorican, France). Sédimentologie, paléontologie, stratigraphie. In *Mémoires de la Societé géologique et mineraligique de Bretagne* (ed H. Lardeux). pp. 183-215.

POTY, E. 2010. Morphological limits to diversification of the rugose and tabulate corals. *Palaeoworld* 19(3–4), 389-400.

RODRÍGUEZ, S. 1989. Lamellar microstructure in Palaeozoic corals: origin and use in taxonomy. *Memoires of the Association of Australasian Palaentologists,* 8, 157-68.

ROUSSEAU, M., LOPEZ, E., STEMPFLÉ, P., BRENDLÉ, M., FRANKE, L., GUETTE, A., NASLAIN, R. & BOURRAT, X. 2005. Multiscale structure of sheet nacre. *Biomaterials* 26(31), 6254-62.

1001 SCRUTTON, C. T. 1997. Growth strategies and colonial form in tabulate corals. *Boletín*
1002 *de la Real Sociedad Española de Historia Natural (Geologia)* 91, 179-91.
1003 SCRUTTON, C. T. 1998. The Palaeozoic corals, II: structure, variation and
1004 palaeoecology. *Proceedings of the Yorkshire Geological Society* 52(1), 1-57.
1005 SEMENOFF-TIAN-CHANSKY, P. 1974. Données nouvelles sur la microstructure de
1006 certains Tétracoralliaires. *Trudy Instituta Geologii i Geofiziki, Mosco* 1, 132-44.
1007 SEMENOFF-TIAN-CHANSKY, P. 1984. Microstructure of *Siphonodendron*
1008 (Lithostrotionidae). *Palaeontographica Americana* 54, 489-500.
1009 SORAUF, J. E. 1984. Upper Permian corals from Timor and diagenesis.
1010 *Palaeontographica Americana* 54, 294-302.
1011 STOLARSKI, J. 2000. Origin and phylogeny of Guyniidae (Scleractinia) in the light of
1012 microstructural data. *Lethaia* 33(1), 13-38.
1013 STOLARSKI, J. 2003. Three-dimensional micro- and nanostructural characteristics of the
1014 scleractinian coral skeleton: A biocalcification proxy. *Acta Palaeontologica Polonica*
1015 48(4), 497-530.
1016 STOLARSKI, J., MEIBOM, A., PRZENIOSLO, R. & MAZUR, M. 2007. A Cretaceous
1017 Scleractinian coral with a calcitic skeleton. *Science* 318, 92-94.
1018 TAYLOR, P. D., KUDRYAVTSEV, A. B. & SCHOPF, J. W. 2008. Calcite and aragonite
1019 distributions in the skeletons of bimineralic bryozoans as revealed by Raman
1020 spectroscopy. *Invertebrate Biology* 127(1), 87-97.
1021 TCHUDINOVA, I. I. 1980. Morphogenesis of Syringoporida. *Acta Palaeontologica*
1022 *Polonica* 25(3-4), 505-11.
1023 TCHUDINOVA, I. I. 1986. Composition, system and phylogeny of fossil corals. Order
1024 Syrlngoporida. *Trudy Paleontologicheskogo Instituta Akademia Nauka SSSR* 216, 3-77.

1025 TOMAŠOVÝCH, A. & FARKAŠ, J. 2005. Cathodoluminescence of Late Triassic
1026 terebratulid brachiopods: implications for growth patterns. *Palaeogeography,*
1027 *Palaeoclimatology, Palaeoecology* 216(3–4), 215-33.
1028 TORNEY, C., LEE, M. R. & OWEN, A. W. 2014. Microstructure and growth of the lenses
1029 of schizochroal trilobite eyes. *Palaeontology* 57(4), 783-99.
1030 TOURNEUR, F. & LAFUSTE, J. 1991. Précisions sur la structure et la microstructure de
1031 *Roemeria bohemica* Počta 1902, espèce-type du genre *Roemeripora* Kraicz 1934
1032 (Tabulata, Dévonien inférieur de Bohême). *Paläontologische Zeitschrift* 65(1-2), 77-
1033 103.
1034 TOURNEUR, F. 1987. *Zemmourella*, nouveau genre de Tabulé du Dévonien moyen du
1035 Zernmour Noir (Mauritanie septentrionale). *Geologica et Palaeontologica* 21, 57-71.
1036 TRIMBY, P. W. & PRIOR, D. J. 1999. Microstructural imaging techniques: a comparison
1037 between light and scanning electron microscopy. *Tectonophysics* 303(1–4), 71-81.
1038 TRULLENQUE, G., KUNZE, K., HEILBRONNER, R., STÜNITZ, H. & SCHMID, S. M. 2006.
1039 Microfabrics of calcite ultramylonites as records of coaxial and non-coaxial deformation
1040 kinematics: Examples from the Rocher de l'Yret shear zone (Western Alps).
1041 *Tectonophysics* 424(1–2), 69-97.
1042 VAN DAALEN, M., HEILBRONNER, R. & KUNZE, K. 1999. Orientation analysis of
1043 localized shear deformation in quartz fibres at the brittle–ductile transition.
1044 *Tectonophysics* 303(1–4), 83-107.
1045 VINN, O. & KIRSIMÄE, K. 201X. *Sphenothallus* (Cnidaria?) in the Late Ordovician of
1046 Baltica, its mineral composition and microstructure *Acta Palaeontologica Polonica*
1047 xx(X), xxx-xxx.
1048 WANG, H. C. 1950. A revision of the zoantharia rugosa in the light of their minute
1049 skeletal structures. *Philos Trans R Soc Lond B Biol Sci* 234(611), 175-246.

Table captions

Table 1: Dimensions of microstructural elements of Syringoporicae from this study in microns.

	Microstructure		Dimensions L		Dimensions F (inn)		Dimensions G		Dimensions F (ext)	
Taxa	**L, F, G**	**Observations**	**Length**	**Width**	**Length**	**Width**	**Length**	**Width**	**Length**	**Width**
***Roemeripora* sp.**	G(F)-L-F	External granular or fibrous domain	x = 12 (8–15)	x = 3 (2–4)	x = 21 (10–38)	x = 2 (1–3)	x = 6 (3–9)	x = 4 (2–6)	x = 20 (9-38)	x = 3 (2 - 6)
Roemeria bohemica	(G)-F-L-F-L-F	Fibrous inner domain match with the septal spines	x = 20 (11-30)	x= 6 (4-7)	x = 31 (18-41)	x = 7 (3-11)	x = 33 (22-51)	x = 19 (10 -29)	x = 27 (13-55)	x = 6 (4-9)
Roemeria cubiniensis	(G)-F-L-F	External lamellar and fibrous domains very thin	x = 19 (11-32)	x = 5 (3-7)	x = 19 (10 - 41)	x = 5 (3-9)	x = 20 (11-40)	x= 11 (8-18)	x = 12 (8-19)	x = 3 (2-5)
Roemeria infundibulifera	(G)-F -L	External fibrous domain very thin or non-existent	x = 29 (13-46)	x= 4 (3-7)	--	--	x=20 (11-33)	x = 13 (8-17)	x = 14 (8-24)	x = 3 (2-5)
Neomultithecopora cantabrica	G-L-F	External fibrous domain very thin	x = 21 (11-43)	x = 7 (4-11)	x = 40 (21-70)	x = 7 (4 - 14)	x = 13 (8-21)	x = 8 (4-14)	x = 15 (9-27)	x = 5 (3-8)
***Pleurosiphonella* sp.**	F-L-F	External fibrous domain very thin or non-existent in halysitid corals	x = 15 (7 - 27)	x = 3 (2 - 4)	x = 14 (8 - 20)	x = 3 (2 - 4)	--	--	x = 25 (14-48)	x = 8 (5-13)

L, lamellae; F, fibres; G, granules; Ext, external; Inn; internal.

Figure captions:

Figure 1. Macroscopic features of the studied coralla in transverse and longitudinal sections. (a-b) Cerioid corallum of *Roemeria bohemica*. (c-d) Cerioid corallum of *Roemeripora* sp. (e-f) Cateniform corallum of *Pleurosiphonella* sp.

Figure 2. Macroscopic features of the studied coralla. (a-c) Phaceloid – cerioid corallum of *Neomultithecopora cantabrica* of Hontoria section. (a) Transverse section incrusting a chaetetid. (b) Longitudinal section of phaceloid part of the corallum. (c) Transverse section of cerioid part of the corallum. (d-e) Phaceloid – cerioid corallum of *Neomultithecopora cantabrica* of Prioro section. (d) Transverse section. (e) Longitudinal section (f-g) Cerioid corallum of *Roemeria infundibulifera*. (f) Transverse section. (g) Longitudinal section (h-i) Cerioid corallum of *Roemeria cubiniensis* (h) Longitudinal section. (i) Transverse section.

Figure 3. Microscopic features of studied taxa. L: Lamellae, μL: Microlamellae, F: Fibres, G: Granules. (a-b) Transverse and longitudinal sections of *Roemeria bohemica*. (c-d) Longitudinal sections of *Roemeria infundibulifera*. (e) Detail of contact of fibrous domain and hyaline elements in a transverse section of *R. infundibulifera*. (f) Detail of contact of fibrous domain and hyaline elements in a transverse section of *Roemeria cubiniensis*. (g-h) Two transverse sections of *Roemeria cubiniensis*. Note the great development of external fibrous domain in (h).

Figure 4. Microscopic features of studied taxa. L: Lamellae, μL: Microlamellae, F: Fibres, G: Granules, Lu: Lumen, Mx: Matrix. (a-b) Transverse sections of halysitid corallites of *Pleurosiphonella* sp. Note the accumulation of matrix over a connecting tubule in (b). (c-d) Transverse sections of *Roemeripora* sp. Note the wavy path of a granular median lamina in (c) and the development of fibres in the median lamina in (d).

(e-f) Transverse sections of *Neomultithecopora cantabrica* in Hontoria section. Cerioid organization in (e) and phaceloid in (f). (g-h). SEM detail of lamellar domain in natural breakage. Note the intralamination smaller than 1 μm that form the crystal (white arrows).

Figure 5. (a-e) AFM images of the nanostructure in *Roemeripora* sp. (a) Amplitude image in the contact of two lamellae (black arrow). Note the nanolamination (dashed line) and the positive relief around nanocrystals. (b-c) Height and phase images of the nanotexture of a microcrystal. Note the intralamination (white arrows) and the nanolaminae that form the structure (dashed line) in (b). (d-e) Detail at high magnification of the dark envelopes of nanogranules (arrows) in amplitude (d) and phase images (e). (f-i) AFM images of the nanostructure in *Roemeria bohemica*. (f) Phase image where the sub-granular nanotexture can be observed in a transverse section of a microcrystal and some areas with nanocrystals fused in large units (black arrows). (g) Height image of a contact between two co-oriented microcrystals. (h-i) Height and phase image of nanotexture of a longitudinal section of a microcrystal. Note the stacking of pill-shape crystals (double black arrow show the morphological axis of the nanounits).

Figure 6. (a-d) AFM images of *Pleurosiphonella* sp. (a) Height image in the contact between two co-oriented microcrystals. Double arrow line points to the direction of co-orientation and white arrow shows an impurity inside the microcrystal. Note the presence of point in contact between nanocrystals (b-c) Height and phase images of the intralamination (black arrows) of the microcrystals. Note as the intralamination is composed of nanolaminae, in which a different phase can be observed around the nanocrystals (dark envelopes) and is thicker in the base of nanolaminae. (d) Note the misorientation between two microcrystals (double arrow lines) and the deep and

continuous contact between them, in contrast with that observed in co-oriented microcrystals (a). (e-h) AFM images of *Neomultithecopora cantabrica* from Hontoria section. (e-f) Height images showing the nanotexture that form the microcrystals. Note the intralamination composed of nanolaminations (white arrows) an the elongated granules. (g-h) Height and phase images of a detail of elongated granules and their co-orientation. Note the dark envelope around the nanounits (white arrow). (i-l) AFM images of *Neomultithecopora cantabrica* from Prioro section. (i-j) Height images of the nanotexture composed of nanolaminae that form the intralamination. (k-l) Height and phase images of a detail of the nanotexture showing the dark envelopes around the nanounits.

Figure 7. (a-c) CIP analysis of an oblique-transverse section of *Roemeripora* sp. in the area between two shared-walls with a granular median lamina. (a) Petrographic micrograph of the investigated area. White arrows point to lamina media. (b) Orientation image of the studied area. (c) Standard colour look-up table (CLUT). I: Pole figure of the entire investigated area. II-III: Pole figures of some areas studied in detail and superimposed to the whole pole figure (lamellar domain and median lamina respectively). (d-f) CIP anaysis of a transverse section of *Roemeripora* sp. in the area between two shared-walls with a fibrous median lamina. (d) Petrographic micrograph of the investigated area White arrows point to lamina media. (e) Orientation image of the studied area. (f) Standard colour look-up table (CLUT). I: Pole figure of the entire investigated area calculated. II-III: Pole figures of some areas studied in detail and superimposed to the whole pole figure (lamellar domain and fibrous median lamina respectively). Black regions in orientation images belong to the thick region of contact between the crystals and opaque impurities and they were not considered for the *c*-axis pole figure calculation. Pole figures were calculated as an orientation distribution

1139 function and provided in multiples of uniform distribution intervals of 0.5 for *c*-axis
1140 orientations. Red points correspond to the punctual *c*-axis orientation of each pixel of
1141 selected areas. These features have been applied to all CIP analysis.

1142 **Figure 8.** (a-c) CIP analysis of a transverse section of *Roemeria infundibulifera* in the
1143 area between two shared-walls with a median lamina composed of hyaline elements. (a)
1144 Petrographic micrograph of the investigated area. White arrows point to lamina media.
1145 (b) Orientation image of the studied area. (c) Standard colour look-up table (CLUT). I:
1146 Pole figure of the entire investigated area. II-III: Pole figures of some areas studied in
1147 detail and superimposed to the whole pole figure (fibrous domain and hyaline elements
1148 respectively). (d-f) CIP analysis of a longitudinal section of *Roemeria infundibulifera* in
1149 the area between shared-walls. (d) Petrographic micrograph of the investigated area.
1150 White arrows point to lamina media. (e) Orientation image of the studied area. (f)
1151 Standard colour look-up table (CLUT). I: Pole figure of the entire investigated area
1152 calculated. II-III: Pole figures of some areas studied in detail and superimposed to the
1153 whole pole figure (lamellar domain and altered area respectively).

1154 **Figure 9.** (a-c) CIP analysis of a transverse section of *Roemeria bohemica* in the area
1155 between shared-walls. (a) Petrographic micrograph of the investigated area. White
1156 arrows point to lamina media. (b) Orientation image of the studied area. (c) Standard
1157 colour look-up table (CLUT). I: Pole figure of the entire investigated area. II-III: Pole
1158 figures of some areas studied in detail and superimposed to the whole pole figure
1159 (fibrous domain and hyaline elements respectively). (d-f) CIP analysis of a transverse
1160 section of *Roemeria cubiniensis* in the area between shared-walls. (d) Petrographic
1161 micrograph of the investigated area. White arrows point to lamina media. (e)
1162 Orientation image of the studied area. (f) Standard colour look-up table (CLUT). I: Pole
1163 figure of the entire investigated area calculated. II-III: Pole figures of some areas

1164 studied in detail and superimposed to the whole pole figure (fibrous domain and altered
1165 area respectively).

1166 **Figure 10.** (a-c) CIP analysis of a transverse section of *Neomultithecopora cantabrica*
1167 in the area between shared-walls of cerioid growth from Hontoria section. (a)
1168 Petrographic micrograph of the investigated area. White arrows point to lamina media.
1169 (b) Orientation image of the studied area. (c) Standard colour look-up table (CLUT). I:
1170 Pole figure of the entire investigated area. II-III: Pole figures of some areas studied in
1171 detail and superimposed to the whole pole figure (lamellar domain and granular median
1172 lamina respectively). (d-f) CIP analysis of a transverse section of *Neomultithecopora*
1173 *cantabrica* of phaceloid growth. (d) Petrographic micrograph of the investigated area.
1174 (e) Orientation image of the studied area. (f) Standard colour look-up table (CLUT). I:
1175 Pole figure of the entire investigated area calculated. II-III: Pole figures of some areas
1176 studied in detail and superimposed to the whole pole figure (altered inner fibrous
1177 domain and altered lamellar domain in contact with matrix respectively).

1178 **Figure 11.** (a-c) CIP analysis of a transverse section of *Pleurosiphonella* sp. in the area
1179 between shared-walls over a connecting tubule. (a) Petrographic micrograph of the
1180 investigated area. White arrows point to contact point between corallites. (b) Orientation
1181 image of the studied area. (c) Standard colour look-up table (CLUT). I: Pole figure of
1182 the entire investigated area. II-III: Pole figures of some areas studied in detail and
1183 superimposed to the whole pole figure (contact area between both corallites and
1184 lamellar domain respectively). (d-f) CIP analysis of a transverse section of
1185 *Pleurosiphonella* sp. of phaceloid growth in a cylindrical corallite. (d) Petrographic
1186 micrograph of the investigated area. (e) Orientation image of the studied area. (f)
1187 Standard colour look-up table (CLUT). I: Pole figure of the entire investigated area

calculated. II-III: Pole figures of some areas studied in detail and superimposed to the whole pole figure (fibrous and lamellar domains respectively).

Figure 12. (a-i) Relative frequency (%) of the correlated misorientation angles in different taxa studied by CIP. Note the variation between those phaceloid taxa (green histograms) and the cerioid taxa (blue histograms). *Roemeripora* sp. (2) correspond with the area studied where appear a fibrous median lamina. *Pleurosiphonella* sp. (2) corresponds with the studied area in a cylindrical corallite.

Figure 13. (a-b) Box charts of length and width sizes of nanocrystals in the different taxa studied by AFM, compared with their morphology. PR: Prioro section, HO: Hontoria section.

Figura 14. Upper part of image shows an sschematic representation of the shared-wall of halysitid corallites of *Pleurosiphonella* sp. and the variation of c-axis orientation around the contact area by the stretching of polyps. Lower part of image shows the variation of morphologies and c-axis orientation of granules and fibres by the folding up of polyps in a cerioid taxon similar to *Roemeripora* sp.

Figure 15. Schematic representation of the passage from cerioid to phaceloid zones into a corallum and their relation with the exposition to waves. The red lines represent the c-axis orientation versus the extinction areas (shadow areas) in each internal structural organization (cerioid, pseudocerioid and phaceloid).

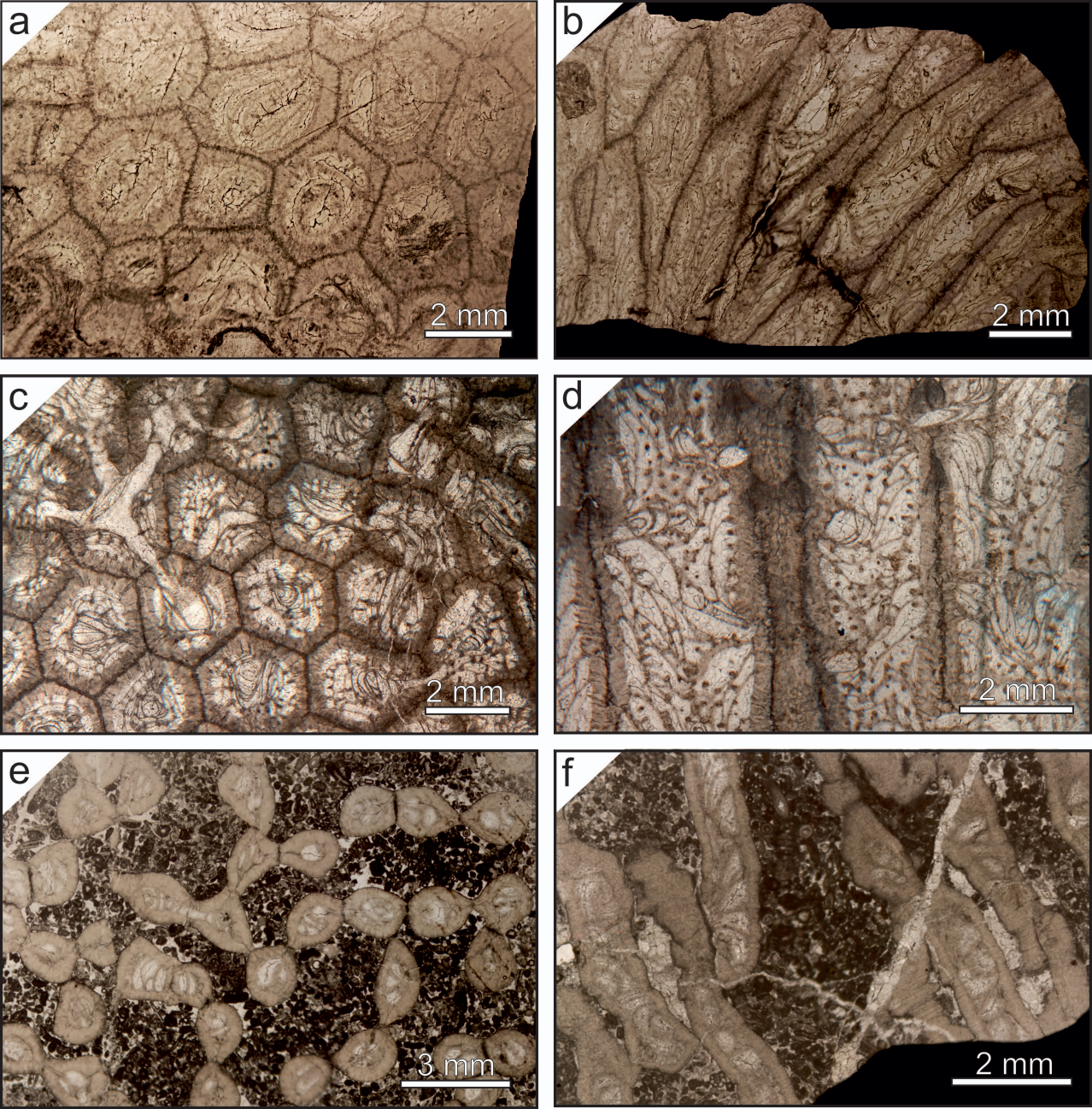
a
2 mm
b
2 mm
c
2 mm
d
2 mm
e
3 mm
f
2 mm

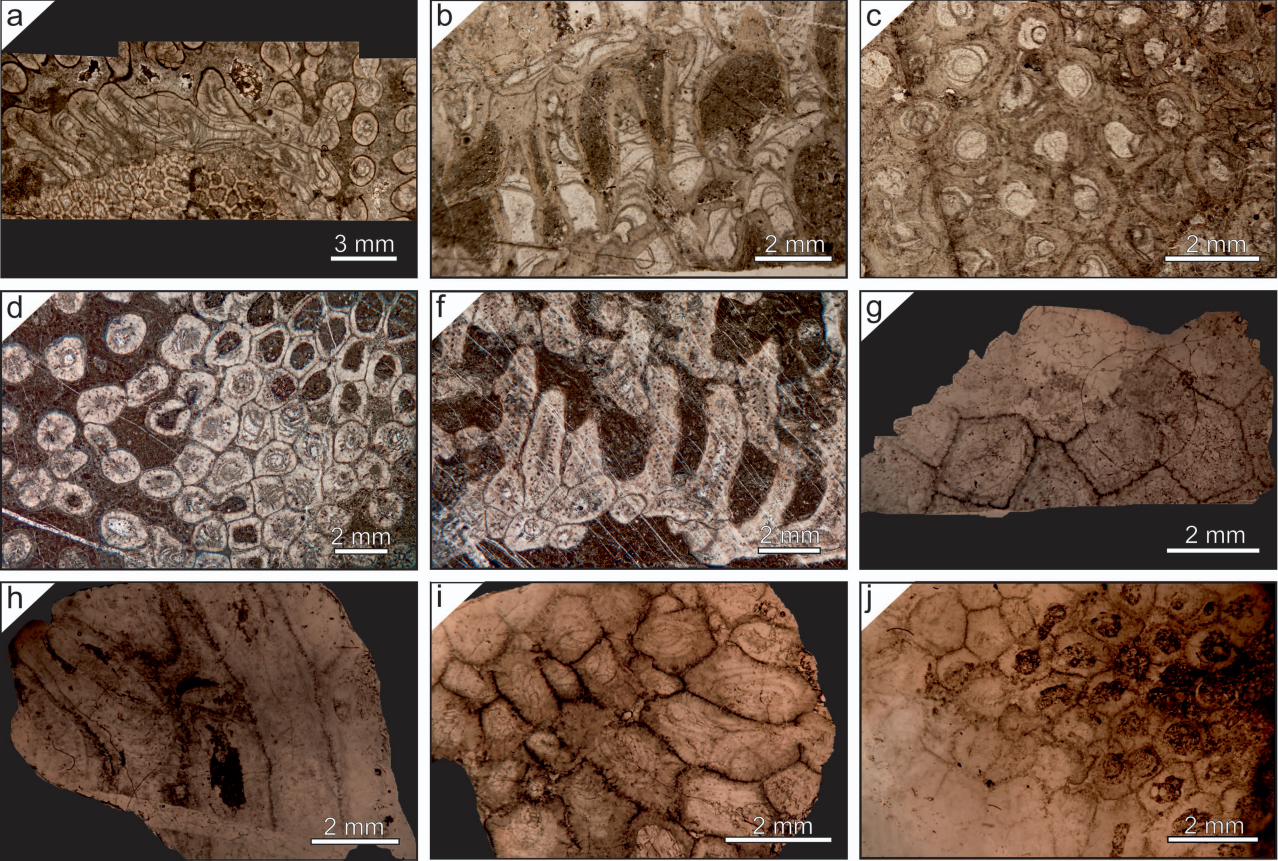
a
3 mm
b
2 mm
c
2 mm
d
2 mm
f
2 mm
g
2 mm
h
2 mm
i
2 mm
j
2 mm

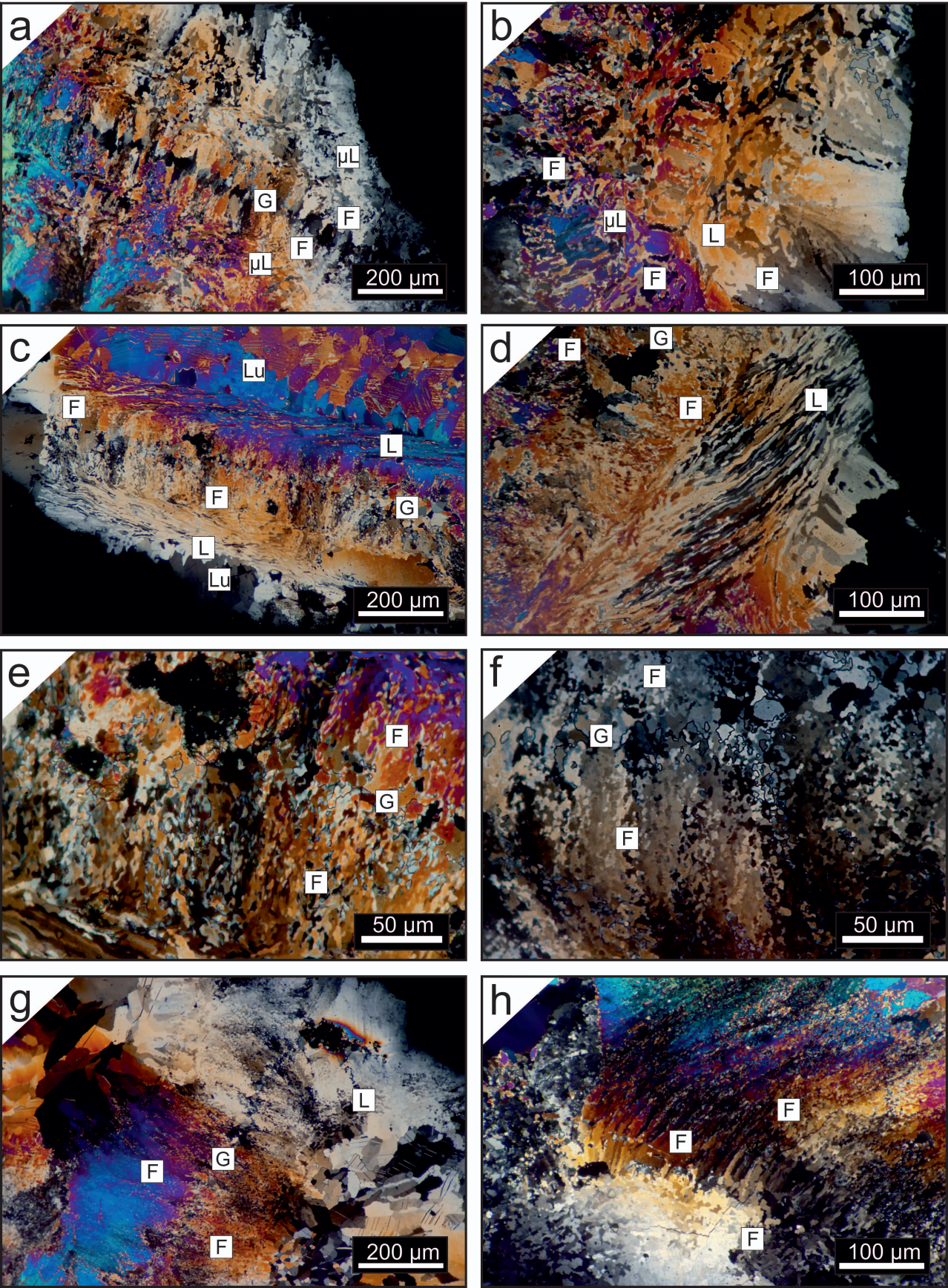
a
μL
G
F
F
μL
200 μm
b
F
μL
L
F
F
100 μm
c
Lu
F
L
F
G
L
Lu
200 μm
d
F
G
F
L
100 μm
e
F
G
F
50 μm
f
F
G
F
50 μm
g
L
G
F
F
200 μm
h
F
F
F
100 μm

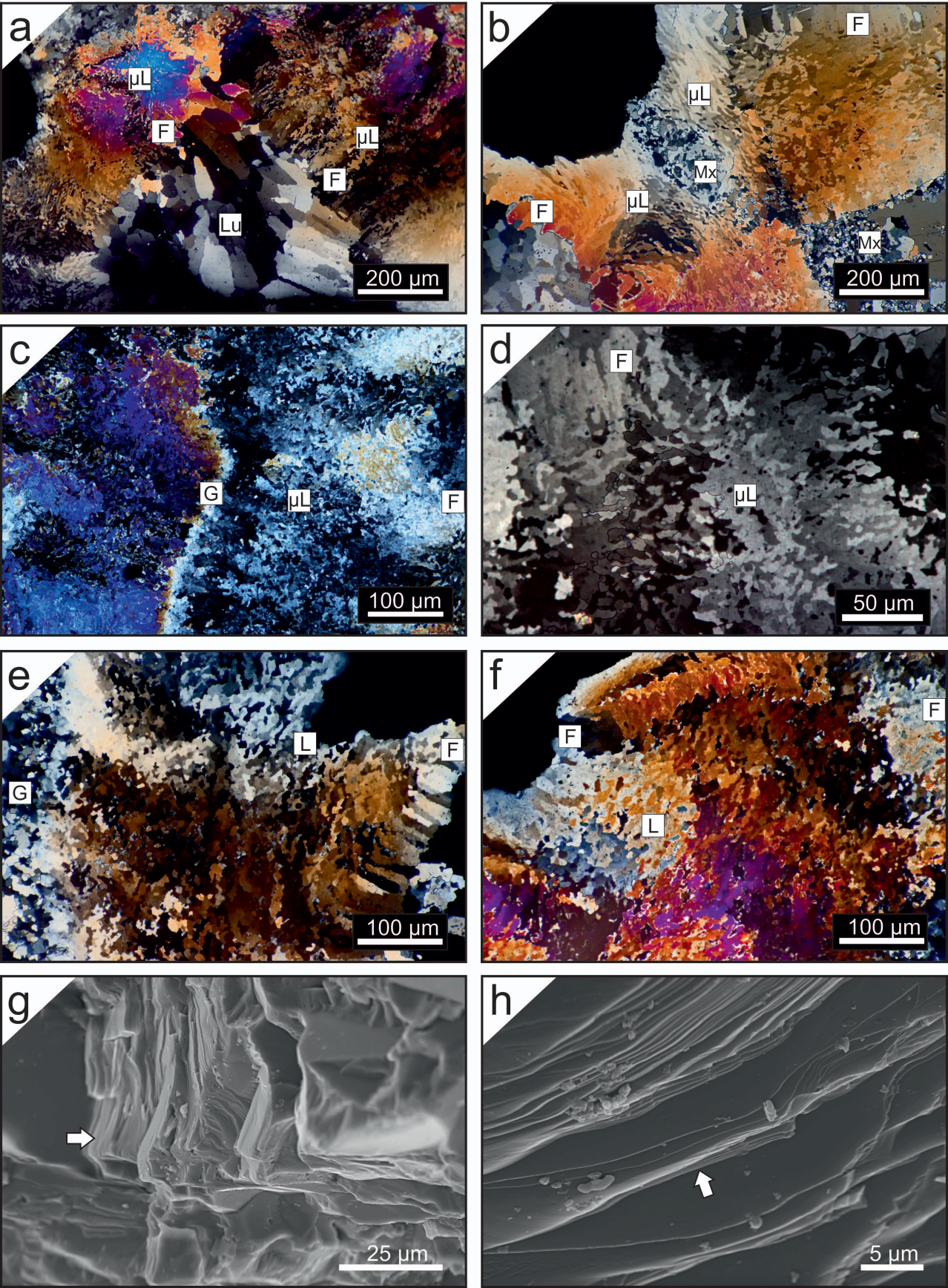
a
μL
F
μL
F
Lu
200 μm
b
F
μL
Mx
F
μL
Mx
200 μm
c
G
μL
F
100 μm
d
F
μL
50 μm
e
L
F
G
100 μm
f
F
F
L
100 μm
g
25 μm
h
5 μm

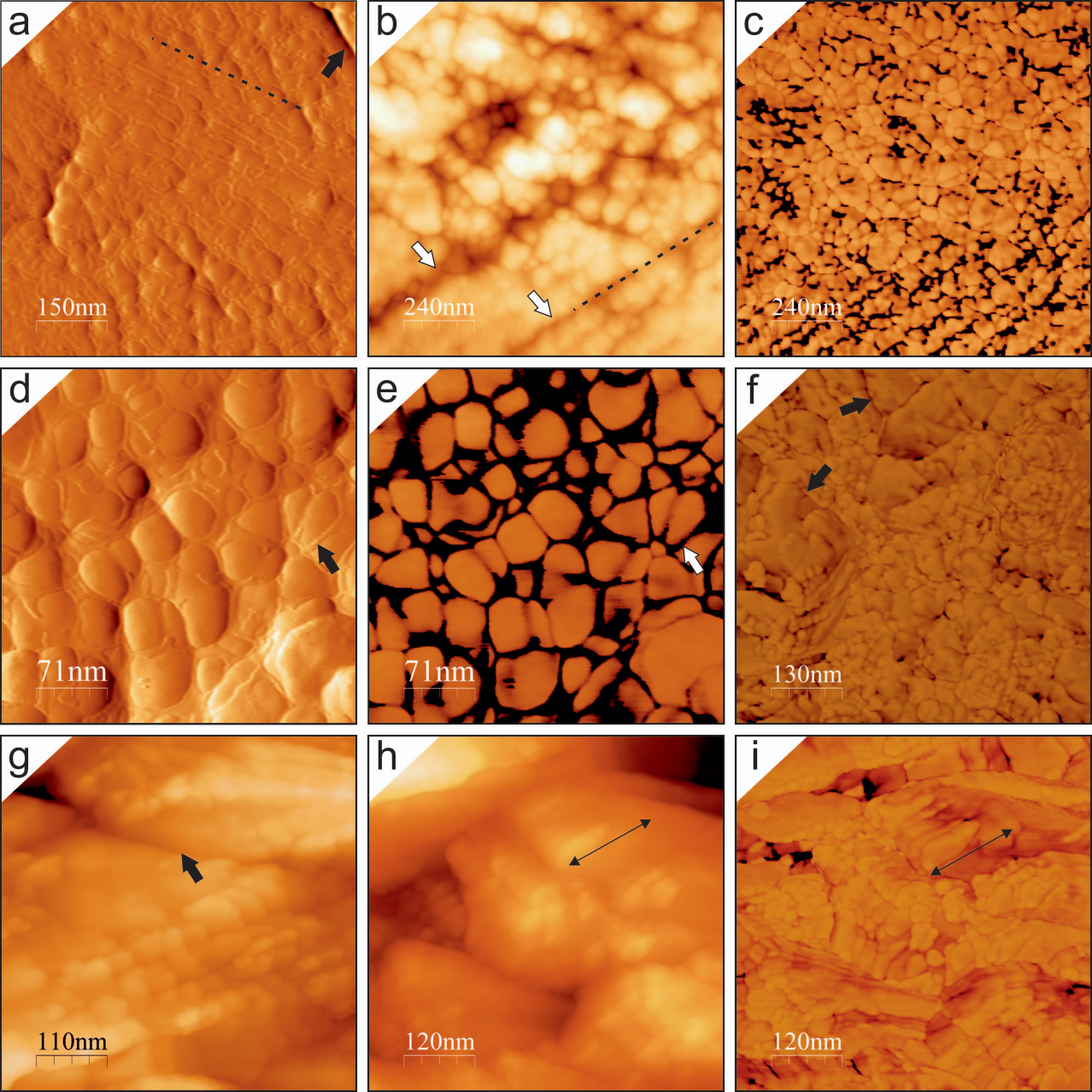
a
150nm
b
240nm
c
240nm
d
71nm
e
71nm
f
130nm
g
110nm
h
120nm
i
120nm

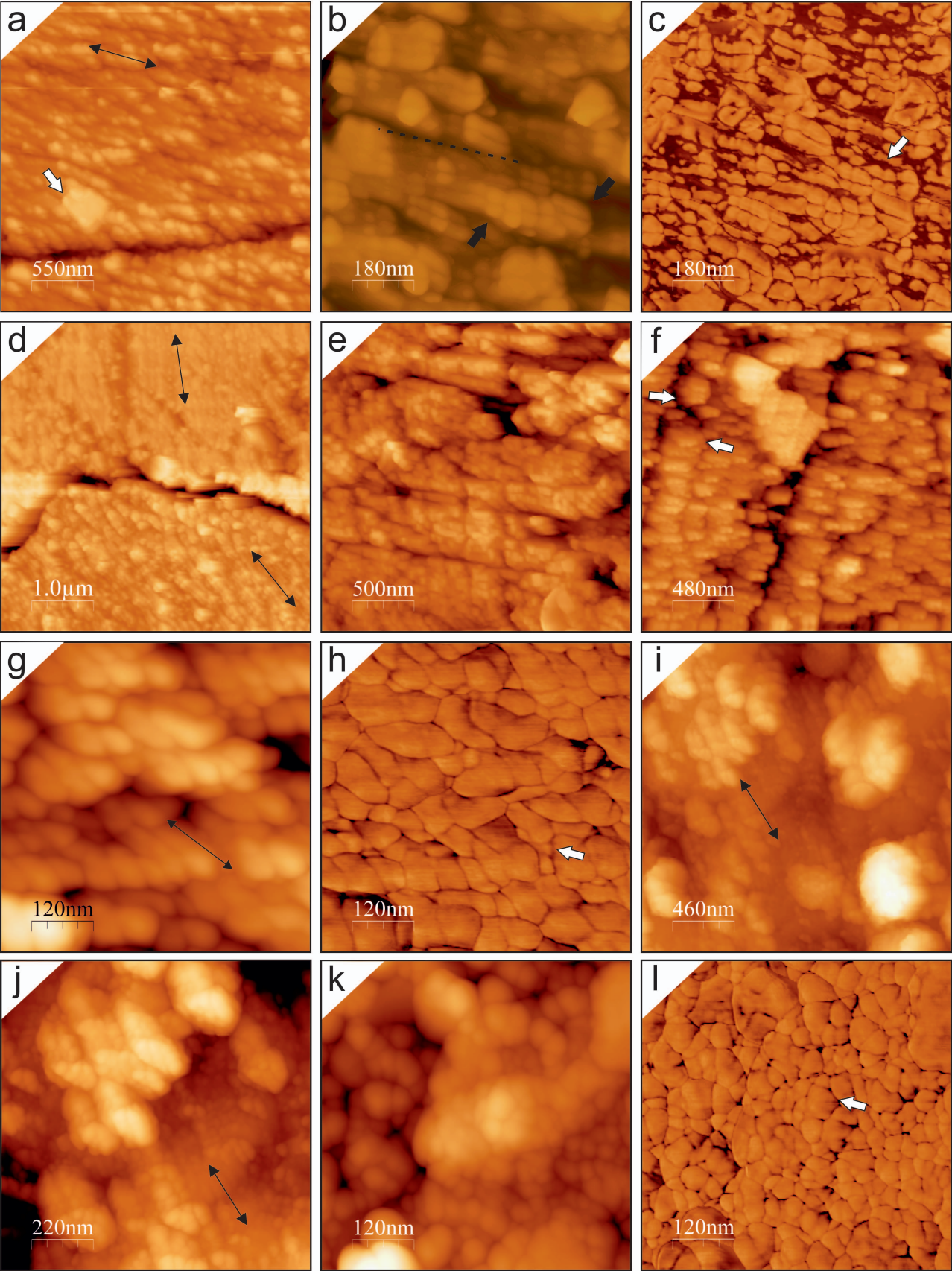
a
550nm
b
180nm
c
180nm
d
1.0µm
e
500nm
f
480nm
g
120nm
h
120nm
i
460nm
j
220nm
k
120nm
l
120nm

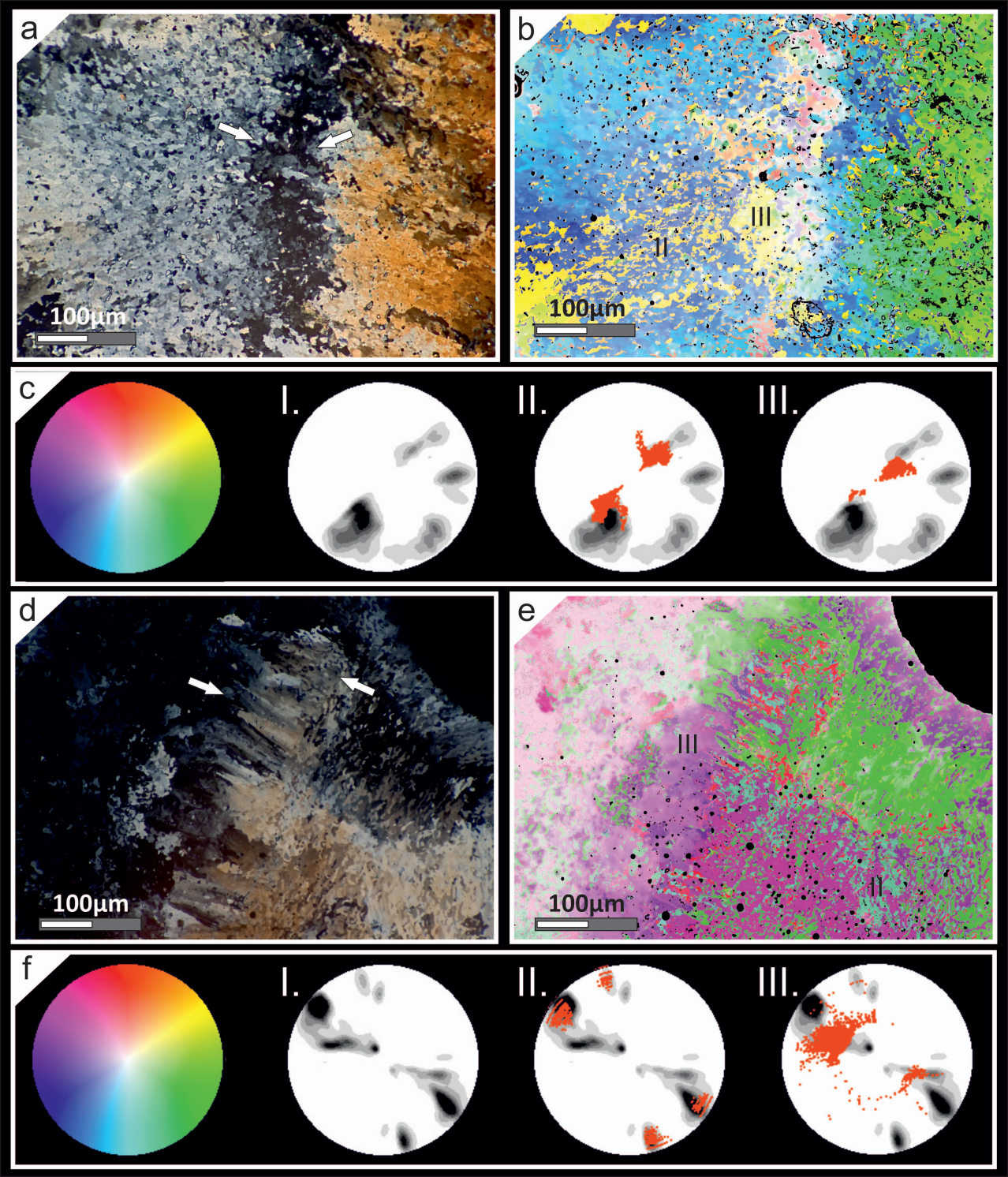
a
100µm
b
II
III
100µm
c
I.
II.
III.
d
100µm
e
III
II
100µm
f
I.
II.
III.

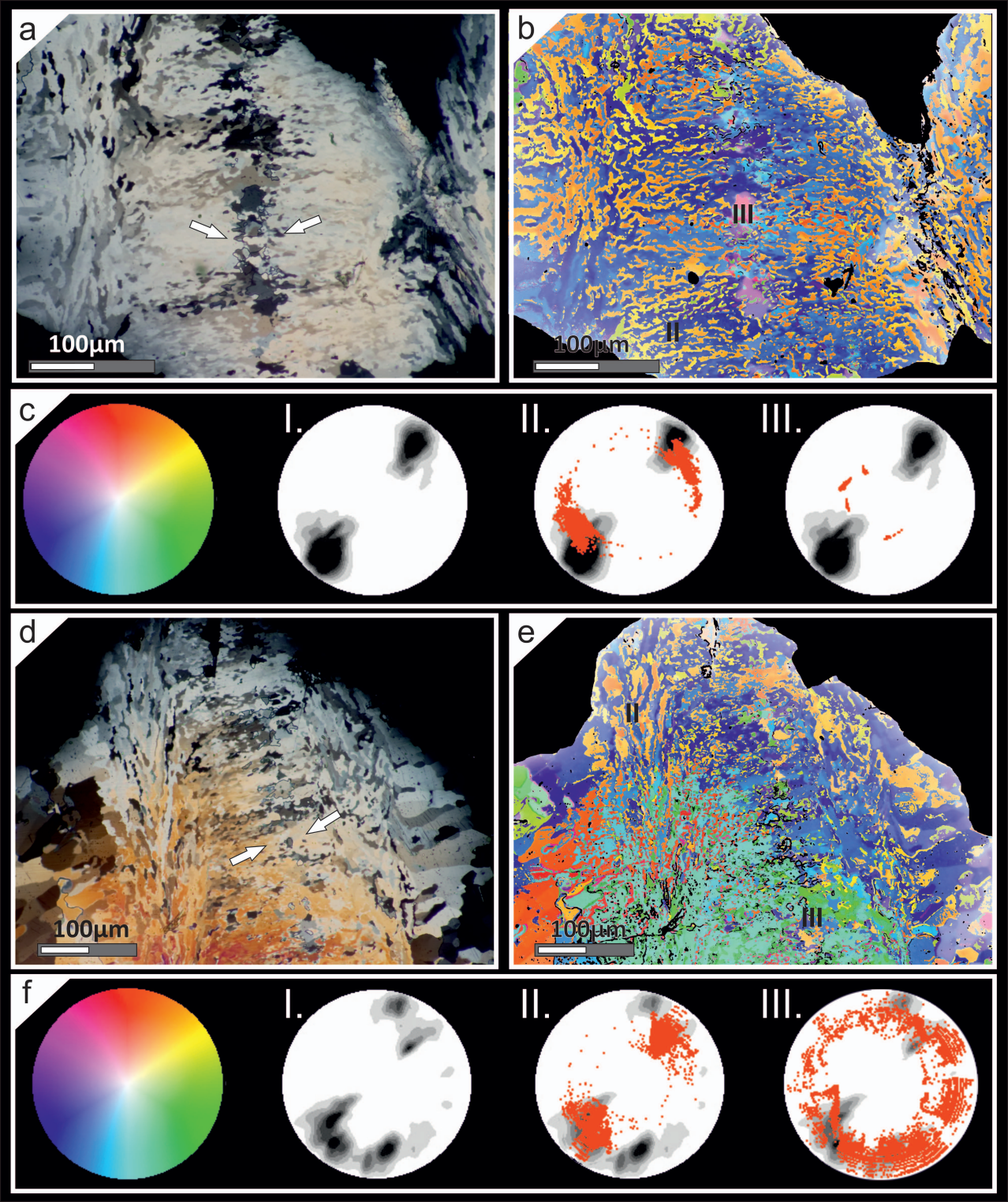
a
100µm
b
III
II
100µm
c
I.
II.
III.
d
100µm
e
II
III
100µm
f
I.
II.
III.

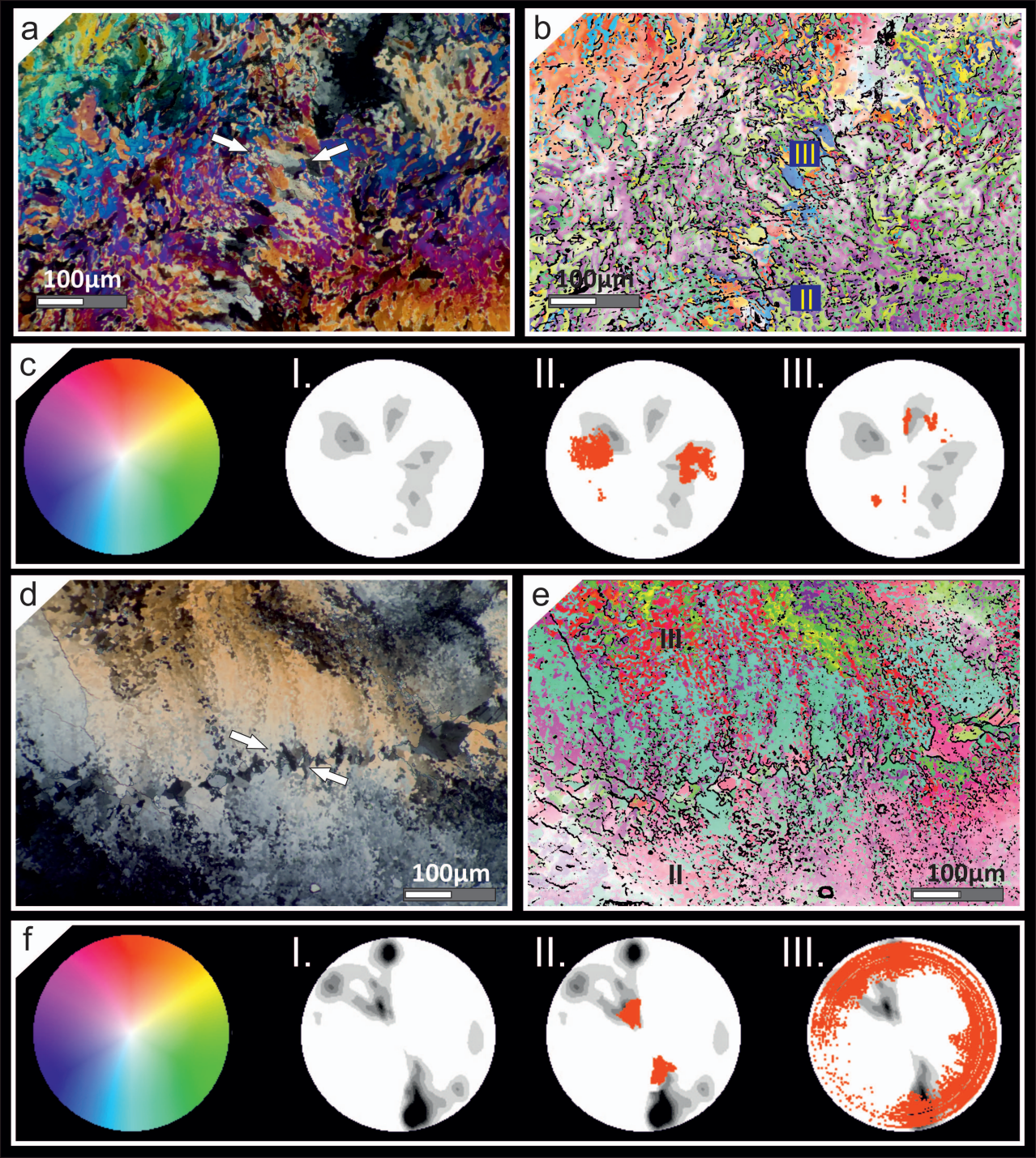
a
100µm
b
III
II
100µm
c
I.
II.
III.
d
100µm
e
III
II
100µm
f
I.
II.
III.

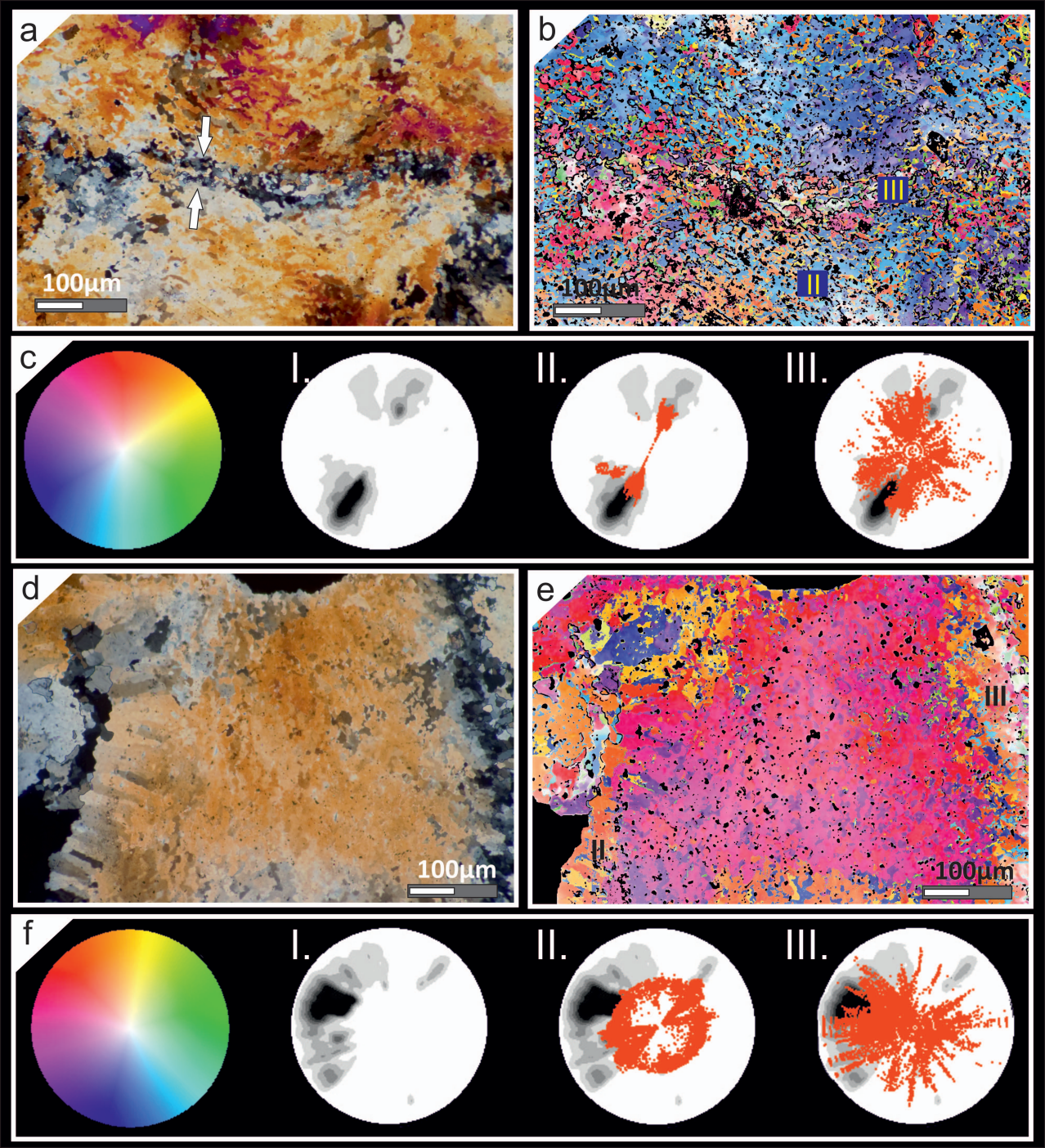
a
100µm
b
III
II
100µm
c
I.
II.
III.
d
100µm
e
III
II
100µm
f
I.
II.
III.

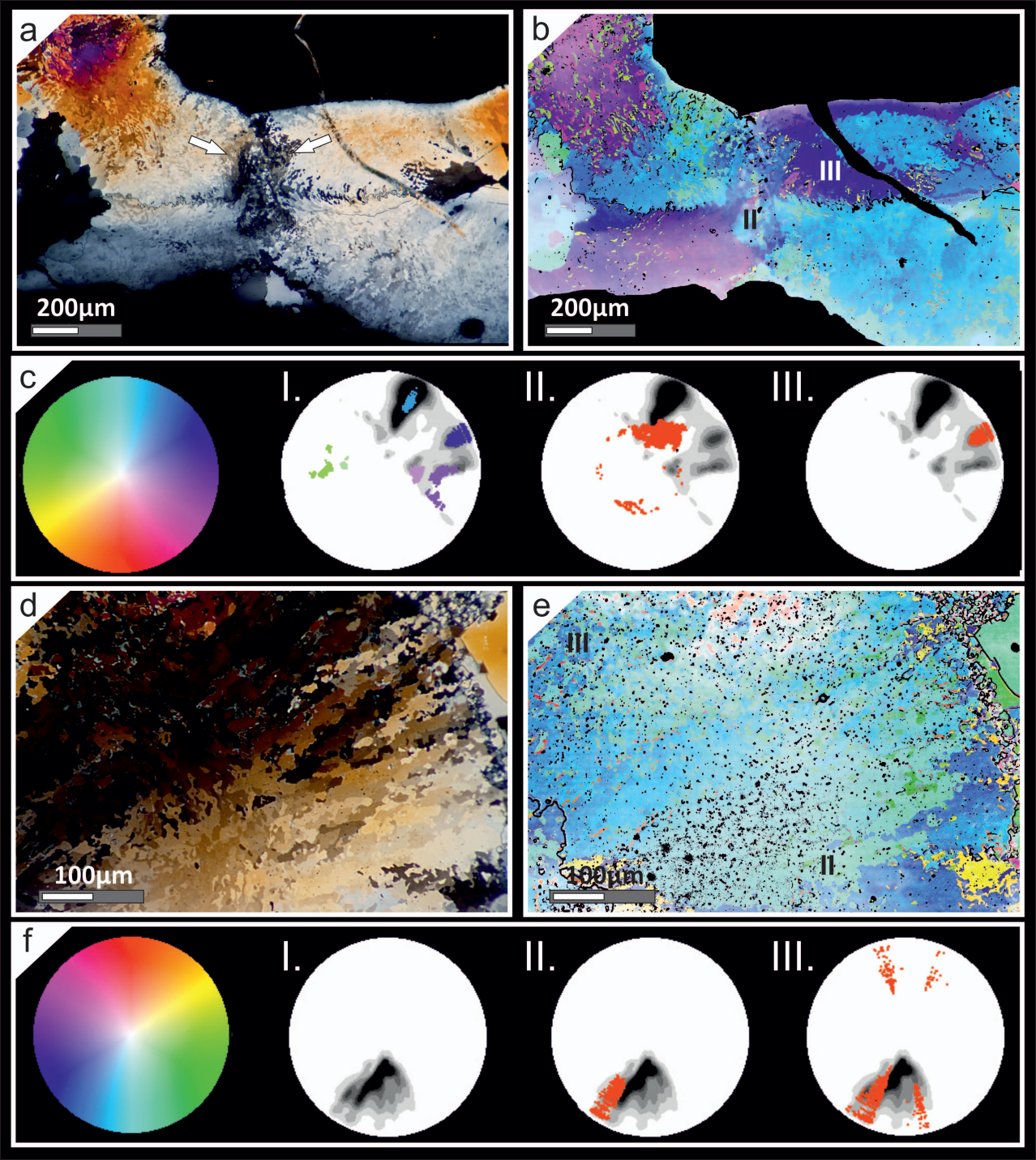
a
200µm
b
III
II
200µm
c
I.
II.
III.
d
100µm
e
III
II
100µm
f
I.
II.
III.

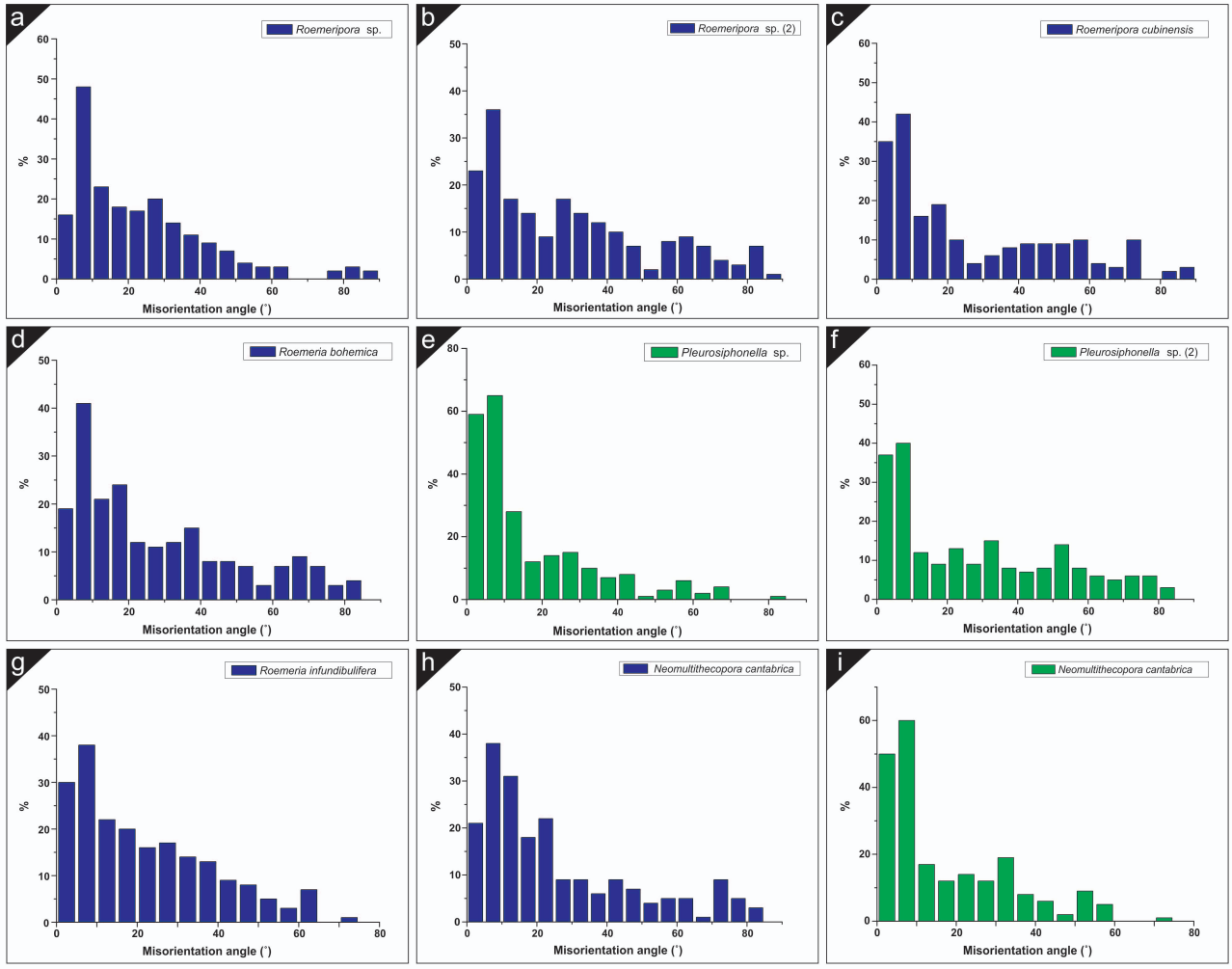
a
Roemeripora sp.
%
Misorientation angle (˚)
b
Roemeripora sp. (2)
%
Misorientation angle (˚)
c
Roemeripora cubinensis
%
Misorientation angle (˚)
d
Roemeria bohemica
%
Misorientation angle (˚)
e
Pleurosiphonella sp.
%
Misorientation angle (˚)
f
Pleurosiphonella sp. (2)
%
Misorientation angle (˚)
g
Roemeria infundibulifera
%
Misorientation angle (˚)
h
Neomultithecopora cantabrica
%
Misorientation angle (˚)
i
Neomultithecopora cantabrica
%
Misorientation angle (˚)

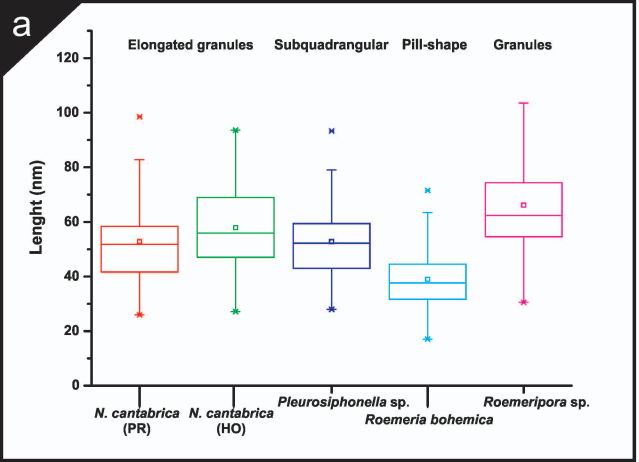
a
Elongated granules
Subquadrangular
Pill-shape
Granules
Lenght (nm)
120
100
80
60
40
20
0
N. cantabrica (PR)
N. cantabrica (HO)
Pleurosiphonella sp.
Roemeria bohemica
Roemeripora sp.

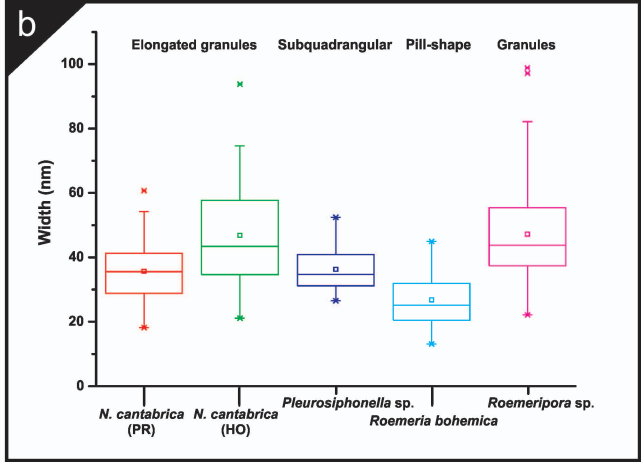
b
Elongated granules
Subquadrangular
Pill-shape
Granules
Width (nm)
100
80
60
40
20
0
N. cantabrica (PR)
N. cantabrica (HO)
Pleurosiphonella sp.
Roemeria bohemica
Roemeripora sp.

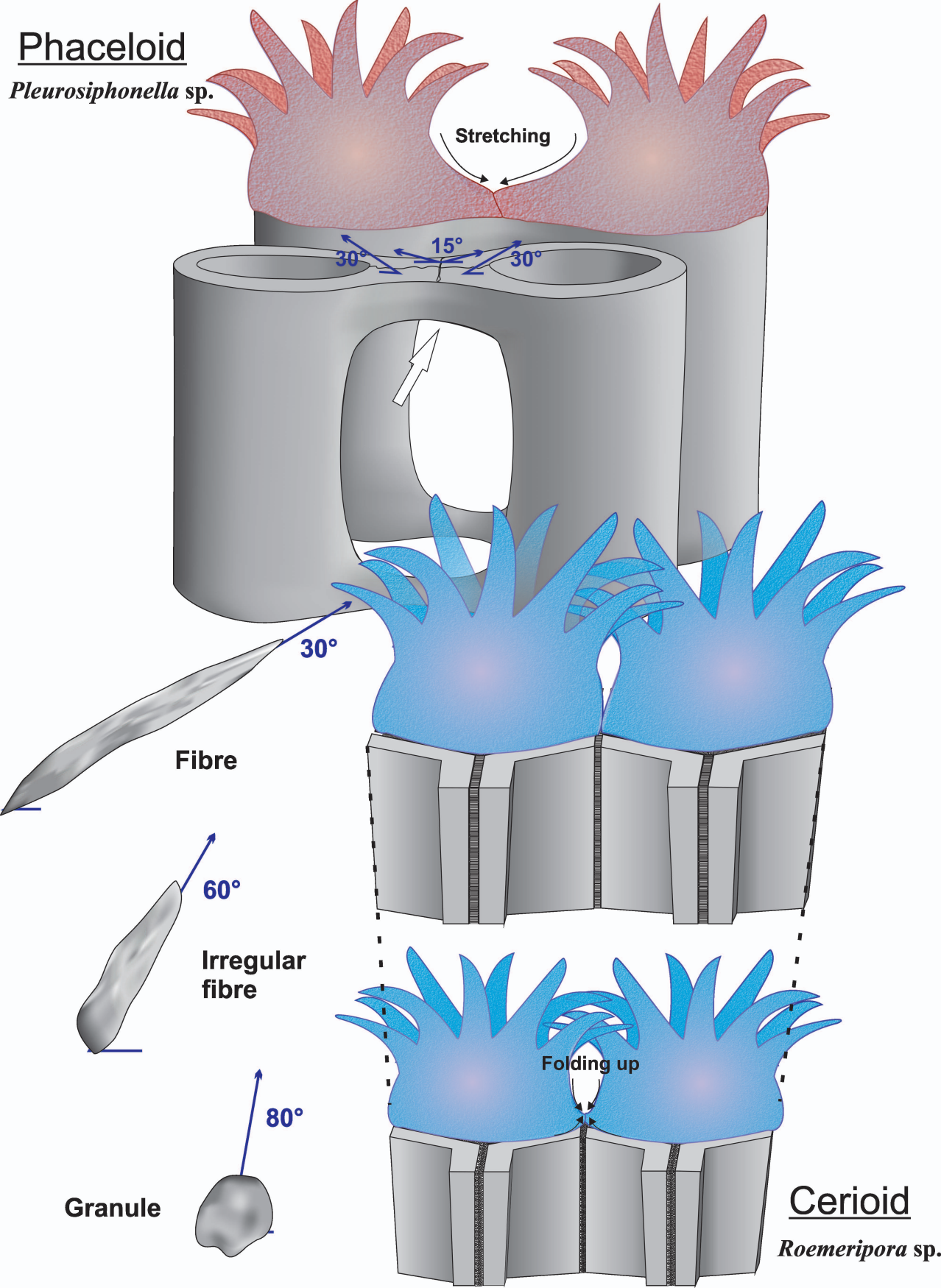
Phaceloid
Pleurosiphonella sp.
Stretching
30°
15°
30°
30°
Fibre
60°
Irregular fibre
80°
Granule
Folding up
Cerioid
Roemeripora sp.

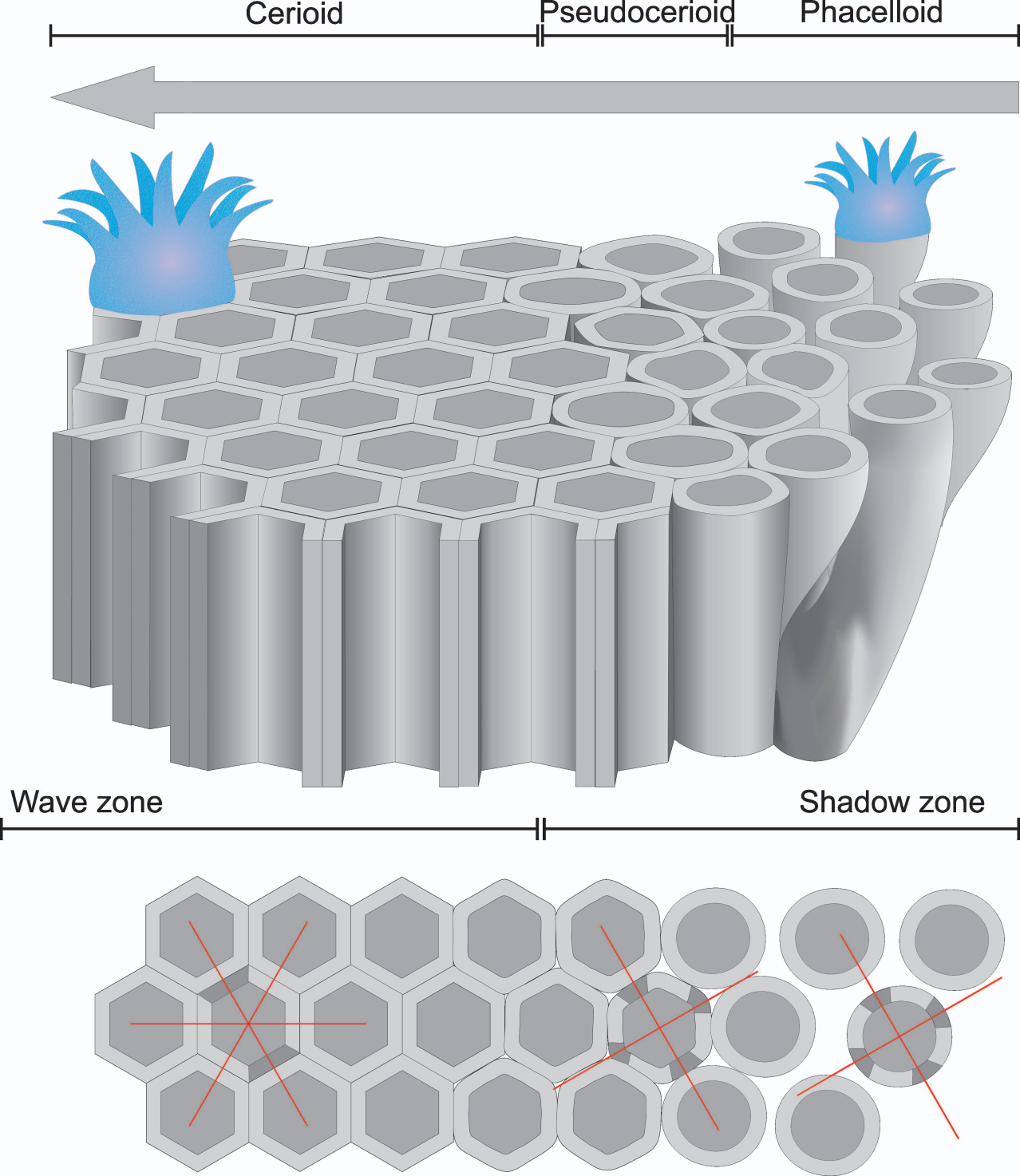
Cerioid
Pseudocerioid
Phacelloid
Wave zone
Shadow zone